Response to reviewer 3

Recommendation to the editor
Thanks for the opportunity to review this interesting paper. I find the topic of the paper of high interest for AMT since it presents an innovative atmospheric measurement opportunity that involves new technology and that requires ad-hoc processing.
However, there are, in my opinion, major deficiencies in the presentation quality that need to be addressed in order to make the suggested measurement technique applicable by other researchers.
Moreover, there are some weaknesses in the scientific reasoning presented that I recommend addressing before publishing. Those weaknesses might not affect the results, but it would be unfortunate to leave incorrect statements on published science that can be misused in the future.

Given the fact that the paper is already under review and the main data is already presented I recommend a major revision and I am definitely willing to contribute again in the review process. However, given the extent of weaknesses of the paper that I will try to list I also encourage the authors to take the time to reformulate the study from scratch and submit a new paper. In either case, I hope my comments will help the authors improving their study.

Authors:
We would like to thank the reviewer for a constructive criticism and suggestions for improving our manuscript. We have tried to respond to all the comments and revised the manuscript significantly. Specifically, we have for the second time substantially revised the manuscript structure, markedly revised the sections related to drop size distribution, and made an attempt to quantify uncertainties influencing our results, which had been previously described rather qualitatively. We have also corrected mistakes, inconsistencies and ambiguities spotted by the reviewer.

GENERAL COMMENTS:

C1) The paper lacks a clear and concise description of the procedure adopted to measure the atmospheric quantities. The concept of baseline and the separation of dry and wet weather is briefly presented at lines 78-82 and does not catch the attention it needs. When I first read the paper I thought that the measuring principle was Eq. 1, but in reality, it is a different formula that involves the concept of baseline (which only partially resembles the components of Eq. 1). The authors have to make a clear definition of dry and wet weather condition (at the moment the reader have to extrapolate from the contest). For dry and wet weather it would be beneficial to have a formula like Eq. 1 that explains how weather conditions influence your measurements (signal loss).

A1: Issue is related to the procedure adopted to measure the atmospheric quantities. Originally, it was described in the method section (lines 230-234 and 297-299). We, however, agree that baseline separation is an important concept which deserves attention. We have, therefore, introduced the concept of the baseline already in section 2.1 (lines 77 - 88) including the formula (originally Eq. 13) and added there also the definition of dry and wet weather:

'Precise separation and quantification of different components of total loss requires detailed description of atmospheric conditions along a CML path as well as conditions influencing hardware of transmitting and receiving stations. The specific path-attenuation due to raindrops or due to water vapor k (dB km^{-1}) is thus usually separated from other sources of attenuation using data-driven approach:

$$k = max\ (\frac{L_t - B - Aw}{l}, 0) \qquad (3)$$

where l (km) is a CML path length, B (dB) is background attenuation, so called baseline, and Aw (dB) wet antenna attenuation (WAA) caused by antenna radome wetting occurring during rainfall or dew events. Baseline is most commonly estimated from attenuation levels during periods without rain and without dew occurrence on antennas (Overeem et al., 2011; Schleiss and Berne, 2010). … We further refer to the periods with and without rain and dew occurrence as wet resp. dry weather.'

The influence of wet weather conditions as a complex issue is described in the following three subsections.
We would like to also note, that section 2 is not intended to describe our original methodology but to provide theoretical background reviewing studies related to CML retrieval of atmospheric variables. The title of section 2 was, therefore, changed to "Retrieving atmospheric variables from CMLs – theoretical background" to stress intended content.

C2) The paper title and abstract suggest that the main results of the study are to use CML to measure rain-rate and humidity. However, in the results section, it is possible to find only an attempt to measure the rainfall rate. Regarding humidity, the paper presents an attempt to estimate microwave attenuation from RH measurements and not the opposite. The results section is filled with arguments about the data processing which do not belong to the results section (wet antenna attenuation, k-R modeling, and gaseous attenuation). It is preferable to put all the data processing in one section and leave the Results section for the atmospheric measurement results and the accompanied estimated uncertainties (that will be of course a consequence of the processing).

A2: We agree that the manuscript (MS) predominantly focuses on the evaluation of rainfall retrieval form E-band CMLs. However, in our opinion, it also investigates the potential of E-band CMLs to observe water vapor. This relies strongly on the ability to separate attenuation due to water vapor from other losses and thus our evaluation focuses on this aspect. The results show that such separation is highly challenging, and, in our view, we state this clearly in the last sentence of the abstract. This is also reason, why we did not proceed further in the quantitative assessment. We would like to also note that we use in the abstract term 'water vapor detection' which, in our view, reflects that water vapor retrieval is not directly quantitatively evaluated. With respect to this issue, we have, however, revised introduction of the method section and section 3.5 describing methodology for evaluating to stress the focus the analysis.

Regarding second concern, variable DSD and wet antenna have been previously identified as one of the most limiting factors influencing CML rainfall retrieval. Quantitative evaluation of these effects was thus in many previous papers considered as a result (e.g. Berne and Uijlenhoet, 2007; Schleiss et al., 2013). We, nevertheless, agree that putting all the data and processing into the Methodology sections and leaving the Result section for the atmospheric

measurement results and uncertainties is reasonable. We have therefore revised the MS accordingly.

C3) The information about methods, data, and results are scattered around and it is very hard to follow the logic of the paper. The authors made an interesting assessment of the ITU k-R relation using PARSIVEL synthetic measurements. I believe that this is an interesting analysis, but it is logically separated from the atmospheric measurement attempts. It might be useful to separate it from the rest making it an entirely separate section (between data and results) or even better would be to include it in what is now section 3.4 making it a self-contained development of the k-R based retrieval technique. Doing that the paper will emphasize the two main atmospheric measurements, namely the dry-weather estimation of water vapor and the wet-weather estimation of rainfall (which includes wet antenna attenuation estimation as a processing step). It would also help to merge section 4 and 5, putting the discussion of the results close to the presentation of them.

A3: We agree, that evaluation of k-R relation using PARSIVEL data can be presented as a self-contained development of the k-R based retrieval technique in one subsection section of the Method section and revised the MS accordingly (section 3.3. in the revised MS). We would keep discussion section separated from the results.

C4) The difficulties in understanding the procedure adopted come also from the fact that not all the variables introduced in the paper are properly defined. Some variable names are reused (c and d are power-law coefficients in section 3 and 4, but where first introduced in section 2 as the speed of light and distance between antennas). Frequency f changes measuring units from Hz at line 93 to GHz at line 96. The definition of dry and wet weather is not explicit, it comes just at the end of the paper from practical considerations. The capped Dm (Eq. 11) is not defined (I think it is the assumed threshold between convective and stratiform events). The separation between stratiform and convective is not described anywhere (it was already question 3 from referee 1); after reading the paper several times I am supposing the threshold Dm is given by an imaginary line in between the two of figure 4b, but this is not written in the paper. Finally, the parameters of the DSD are reported in Tab. 3, but they are not explained (already question 5 from reviewer 1).

A4: The variable names in the revised MS have been unified and units properly defined. The definition of dry-wet weather is introduced earlier (see answer A1)

Capped Dm is estimated based on disdrometer data and its definition and estimation procedure was described at lines 265-270 of the original MS. Suggested revisions further clarifying the procedure are discussed in the answer A8.

The parameters introduced in table 3 were explained at bottom line of the table only. In the revised version of MS, reflecting criticism in C8, we have decided to remove analysis with theoretical DSD functions.

C5) Some comments appear to come out more from wishful thinking than from a proper quantitative evaluation of the results. As an example in lines 442-446 the uncertainties related to WAA and DSD assumptions are discussed only in a qualitative way. The authors missed the opportunity to quantify the uncertainty related to WAA to RR estimation as a function of link length. Alternatively, by analyzing the k-R scatterplot of the Prague data one could potentially make some quantitative assessment of the RR retrieval uncertainties due to DSD

assumptions (the underestimation of RR below 2 mm/h is a very interesting aspect related to this).

A5: We made an attempt to estimate quantitatively uncertainties of CML QPEs and uncertainties related to WAA and DSD. The methodology of uncertainty estimation is now described in the method section and estimated uncertainties are presented together with the results (section 4.2). The updated evaluation indicates that underestimation of RR below 2 mm h^{-1} might be indeed related to DSD as it corresponds quite well to expected underestimation of the ITU-based k-R model during stratiform rainfalls (Figure 10 of the revised MS and also Figure R3 in answer A25).

SOME CONCERNS ON THE FIRST REVIEW:

C6) During the review process, the CML sub-link naming scheme changed. This modification makes sense since it simplifies the naming scheme, but I do not see in the author's response a mention to this change. Also, the naming change seems not consistent: link 3008-3009 became link 6 in the map of figure 3, the same link in table 1 became link 3 (but I see that there is a reordering problem here), but again in figure 10 the cluster of data point that was previously from 3008-3009 are now belonging to the subplot of link 3. I suggest mentioning all the changes made to the manuscript in the ``answers to the reviewers'' documents, also the ones that have not been suggested by the reviewers.

A6: This change was reported in the response to the referee 1, specifically response to the comment no. 3. We have decided to reorder the IDs to reflect link length. Reordering, in our view, improves clarity of the section quantifying WAA, where effect of CML path length on total attenuation is demonstrated. However, we made mistake in Figure 10 (Figure 6 in the revised MS). The mistake is corrected and all the figures are now consistent with the new naming.

C7) I wasn't able to find the details of the T-matrix simulations in section 3.5 as the authors answered comment 2 by Dr. Guyot. Actually, I wasn't able to find those details anywhere in the manuscript. I suggest to include the T-matrix parameters information and to move it to section 2 (not 3.5 as the authors mentioned), this is because the T-matrix parameters are essential to reproduce the results of figure 2.

A7: Thank you for spotting this inconsistency. We have added the details on T-matrix simulations into the revised MS to section 3.3 at lines 245-248, as the parameters of the T-matrix simulations are integral part self-contained development of the k-R based retrieval technique. Moreover, the paragraph explaining extinction-efficiency as well as figure 2 were removed (see A18).

A8) The answers of the authors to reviewer 1 (questions 5 and 6) are not addressing the reviewer's concerns. Probably the authors misunderstood the questions since they briefly refer to Ulbrich (1983) to cover the entire discussion, but the points remain unanswered. Moreover, the phrasing used in both the manuscript and the answer is imprecise and leads to a misunderstanding of Ulbrich (1983) findings.
In Ulbrich (1983) it is assumed that any DSD is well represented by a three-parameter modified-gamma distribution. This assumption leads to the conclusion that every couple of moments of the DSD can be related through a power-law. Because of that, if one can

characterize a couple of moments through a power-law it follows that the DSD becomes a 1-parameter only function (the free parameter is lambda) and any other couple of moments will be characterized by a corresponding power-law. For this reason, the reflectivity-rain rate fits of Fujiwara (1965) can be converted into fixed parameters N0, mu for the DSD and power-law coefficients epsilon-delta for the Dm-RR relation.
There are many problems with this approach:
- All the assumptions of Ulbrich (1983) have to be valid. The authors did not test, for example, how good a modified gamma with fixed N0 and mu parameter fit the DSDs measured by PARSIVEL
- The error in the Z-R fit are not evaluated and transferred to errors in the N0, mu, or Dm as computed by the implied Dm-RR relation

- The mathematical foundations of Ulbrich (1983) have been demonstrated to be flawed in logic (Illingworth and Blackman 2002), leading to artificial correlations among parameters.
To the best of my understanding, the theoretical DSD is used only to make a rough evaluation of the stratiform or convective nature of the precipitation in the PARSIVEL dataset. I do not think it will affect the results, but the explanation of how to use the theoretical DSD has to be corrected anyway.
What it comes out from these considerations and might be harder to sustain is the following: ``The k-R function (stratiform DSD) applied to the Prague dataset has been estimated from a fit to synthetic data obtained from the Duebendorf dataset (13 months) whose stratiform-convective classification is based on the distance of the data from the Dm-R curves derived with a mathematically faulty logic (Ulbrich 1983) using reflectivity-rain rate fits obtained by observing 31 storms in Florida (Fujiwara 1965)."
This argumentation looks weak to me and I wonder if the authors excluded any other possible option they had to discriminate between stratiform and convective cases in the Duebendorf dataset.

A8: This is really interesting point. We were not aware of the shortcomings of Ulbrich (1983) parametrization and indeed did not interpret concerns of the reviewer 1 in this respect. We, therefore, suggest removing analysis with theoretical pdfs of drop size spectra (it was already suggested by reviewer 1) and keep only analysis with DSD from the PARSIVEL dataset.

Regarding rainfall type classification, we would like to note, that we aim at distinguishing between rainfalls based on their drop size spectra, rather than classifying nature of precipitation. In the revised MS, we explicitly state this in the introductory of section 3.3 (lines 242-244): 'The investigation is performed on PARSIVEL observations of DSD from Duebendorf dataset. The classification of rainfalls based on their mass-weighted diameter is introduced to enable optimization of k-R model separately for rainfalls with different drop sizes.'
We have also changed explanation of classification procedure on lines 261-263 and hopefully, more clearly state in the revised MS that the classification evaluates nature of the precipitation only roughly: 'D_m-based classification separate rainfalls by size of their raindrops to two classes and thus also roughly evaluates convective and stratiform nature of the precipitation in the PARSIVEL dataset (Jaffrain and Berne, 2012). We further refer to those two classes as 'stratiform' and 'convective'.'
The mass-weighted diameter (or median volume diameter or other DSD moment ratio) is in our view appropriate descriptor enabling such classification. Relating the capped D_m

threshold to rainfall intensity is consistent with our data and also with some other studies, e.g. Meshesha et al. (2014).

The power-law relation between DSD descriptor and rainfall intensity was optimized using the whole Duebendorf (PARSIVEL) dataset (described originally at L270-271). We have revised this description (lines 259-265 in the revised MS) as follows: 'Parameters γ and δ are estimated by fitting Eq. (11) to D_m as derived from PARSIVEL records using Eq. (10). Specifically, sum of squared residuals between D_m obtained from Eq. (10) and Eq. (11) is minimized. This results in parameters γ = 1.29 mm $mm^{-\delta}$ h^{δ} and δ = 0.16.'

We have tested this approach for different moment ratios and also for median volume diameter (D0) (fig. R1). All the power-law fits result in similar number of rainfall records classified as stratiform (62 -65 %) and convective (35-38 %) and except the lowest moment ratio, most of the high intense records are classified as convective.

We have also tested how the classification, based on different DSD moments + median volume diameter, influence k-R power-law model when optimized separately for records stratiform and convective rainfalls (fig. R2). The power-law fits for convective rainfalls are similar for all the classifications except the one using the lowest order moments. For stratiform rainfalls, differences appear especially for rainfall intensities higher than approx. 7 mm / h. Classification using higher moment orders result in steeper k-R curves (higher R for given k). An exception is the lowest order moment ratio (M1/M0), which classifies records with high intensities into the stratiform group and thus seems to be inappropriate for such classification.

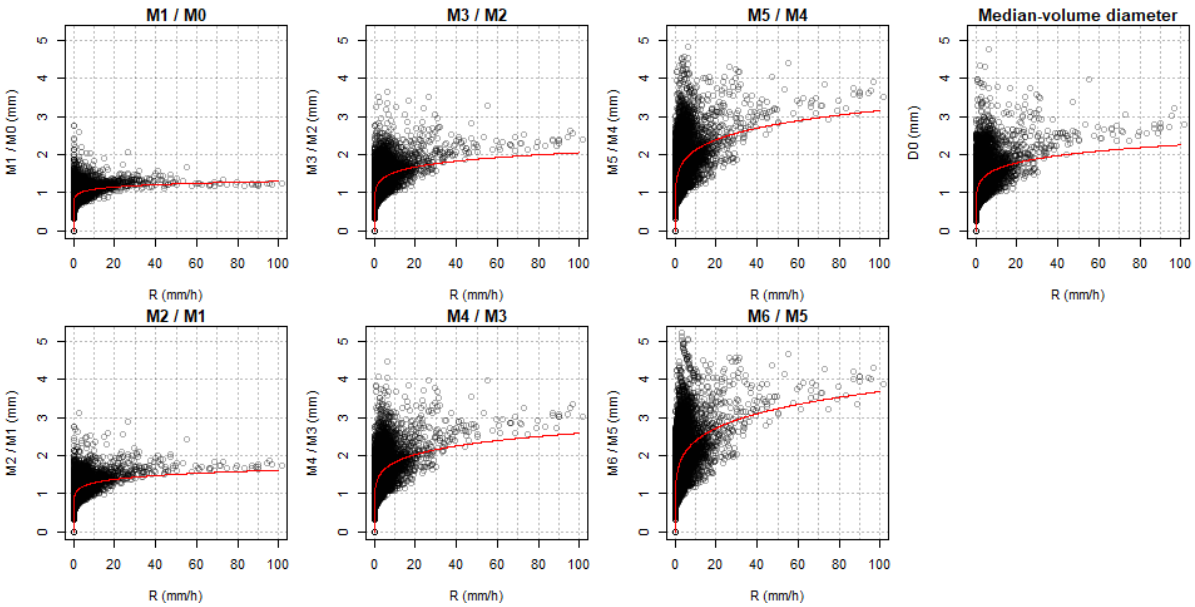

Figure R1: Power-law fits between rainfall intensity and different moment ratios quantified from DSD observed by PARSIVEL disdrometer.

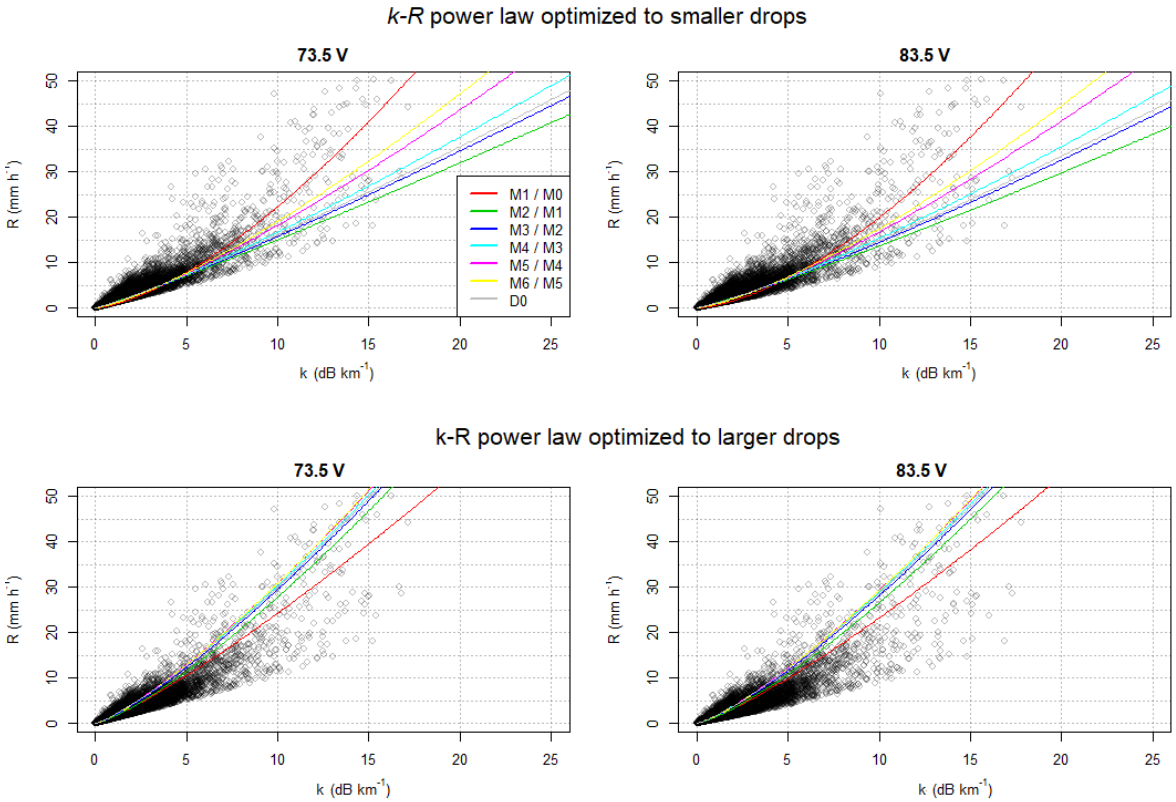

Figure R2: k-R power law relation for vertically polarized 73.5 and 83.5 GHz plane wave fitted separately to rainfalls classified as stratiform (top) and convective (bottom). The classification uses different DSD moment ratios and median-volume diameter.

With respect to the last concern, we have to note that disdrometer observations which would enable classifying rainfalls based on their drop size spectra are not available for Prague dataset. We are, however, convinced that assuming drop size spectra with smaller mass-weighted diameter during Autumn period is reasonable in the climate of the Czech Republic. In addition, the uncertainty analysis, which is presented in the revised MS, supports our conclusion that the effects of DSD is significant for the longest CML and that reported improvement in QPEs is likely due to k-R model optimized for PARSIVEL records classified as stratiform.

C9) A very minor point on comment 2 from reviewer 1. By looking at the figure and its caption I also get the wrong message that there is a drop in the water vapor attenuation around 60 GHz. The detail of k being defined differently for Oxygen and Water is not clear from the figure. If I just look at it, I see that a certain concentration of water vapor absorbs the plotted amount of energy which depicts a dip around 60GHz that shouldn't be there. One way to make the figure less prone to misinterpretation is to define the a) subplot y axes as k_moist - k_oxygen, this reflects the description added to the text and conveys a clear message.
Another option is to plot the attenuation only for the frequencies of interest for the paper 70-90 GHz. The rest of the spectrum is not needed since it is not utilized or even discussed as a comparison to lower frequencies CMLs. In this case, I would also avoid plotting the b) panel altogether since it is not used in the paper.

A9: Agreed. We have modified the figure as suggested in the first paragraph. We only prefer to use k_dryair instead of k_oxygen, because the dry-air attenuation includes also attenuation by nitrogen.

We would like to keep the panel b in this figure, as dry-air attenuation influences also losses on 73.5 and 83.5 GHz, i.e. frequencies evaluated in our results.

MORE SPECIFIC COMMENTS:

C10) Equation 1 -It may sound trivial, but I suggest to introduce the definition of Lt as tx -rx, so that the equation becomes Lt = tx - rx = Lbf + Lm + ...

A10: Agreed (see line 66).

C11) Line 48 - I do not know if the term resonance peak in parentheses can be considered correct. I would avoid it.

A11: Agreed.

C12) Line 73 and following - There is some confusion among the use of the terms loss, attenuation and specific attenuation. Perhaps it is better to clear in the introduction that in general, in the text the term attenuation refers to specific attenuation (dB/km) apart from WAA where it actually means loss (dB).

A12: Agreed. We have clear at the end of the subsection the usage of these terms: "We further use the term loss when referring to reduction in power density of EM wave in dB, whereas the term attenuation mostly refers to specific attenuation (dB km^{-1}) apart from WAA where it actually means loss (dB). We, nevertheless, stick to the term WAA as it is already established in literature."

We also present in the revised MS results of gaseous attenuation analysis in dB km^{-1}. In addition, when quantifying WAA we use in the revised MS the term total rainfall-induced loss, instead of to total attenuation.

C13) Line 112 - also polarization and orientation of the drop is relevant (if the drop is not considered spherical)

A13: Agreed. We have modified the sentence as follows: "Attenuation caused by a single raindrop is determined by the wavelength, polarization, refractive index of water, shape parameters of the raindrop and its orientation."

C14) Line 114 - How is D defined? From the typical usage of the pytmatrix package and Eq. 6 it only makes sense that this is the equivalent-volume diameter. Does this definition match the size measured by the PARSIVEL disdrometer?

A14: Yes, it is equivalent volume diameter. We have specified this after the equation in the revised MS (L129). Although PARSIVEL disdrometer measures particles up to 25 mm we consider only particles with diameter from 0 to 5.5 mm to be raindrops. The definition (and calculation of extinction cross-section) is appropriate for this range of diameters.

We have added information on drop size range into section 3.1 of the revised manuscript where PARSIVEL (Duebendorf) dataset is presented (lines 180-181): "Particles larger than 5.5 mm are not considered to be raindrops and thus excluded from the analysis."

C15) Line 115 - The contribution of secondary waves is commonly referred to as "multiple scattering" effects; I think the authors can use this term to simplify the discussion. Anyway, the argumentation on why multiple scattering is negligible is wrong.
Usually, the evaluation if multiple scattering has to be taken into account, is done in terms of optical depth (Battaglia 2006). Optical depth takes into account the scattering intensity through Cext, and particle number concentration Nt. Even assuming Cext to be not relevant what becomes important is not N(D) which is the drop density per size bin, but the total drop density Nt=int N(D)dD.

A15: Thank you. We have reformulated the text to: "The total drop density in the unit volume N_t *(*m^{-3}*) is relatively small for natural rainfalls. Therefore, the multiple scattering effects can be neglected."*

C16) Line 119 (Eq. 5) - I believe there is an error in the formula. If Cext is cm**2 I think the coefficient at the beginning of the formula should be 0.4343 and not 4343.0 (Berne and Uijlenhoet 2007)

*A16: Indeed, it should be either 0.4343 or Cext should be in m**2. Thank you for spotting this mistake, we have corrected it.*

C17) Line 122 - Saying that R and k are equal to moments of the DSD implies that v(D) and Cext(D) are power-laws. This is a reasonable assumption for small drops for which the Stokes approximation of drag force can be assumed and the Rayleigh approximation for scattering applies, but it is not true in general (as it can be seen from Fig. 2 for drops larger than 1 mm). Also, the authors should change the term "equal" with the term "proportional to". As a matter of fact, if the two quantities would be always proportional to a moment of the DSD the relation between the two would be linear and not a power-law (that is what happens at lower frequencies).

A17: Thank you for this explanation. We have decided to simplify the sentence and remove statement about moments, instead we refer to Olsen et al., (1978): "The relation between attenuation and rainfall intensity can be approximated by a power-law (Olsen et al., 1978):"

C18) In Figure 2 and Eq. 9 it is introduced the concept of extinction efficiency, but this is of no use for the application of the proposed study. The important quantity that goes in Eq. 5 is Cext, not Qext. This analysis leads to another wrong statement at line 139. A single large drop contributes much more to attenuation than a single small one.
On the other hand, it is relevant for the study to analyze the relative attenuation of DSDs with small and large Dm and the same RR. In these conditions, it is true that large drops attenuate less because they produce smaller attenuation per unit mass (not per unit area). Also, larger drops fall faster, meaning for the same RR their volumetric concentration is lower.

A18: Thank you, we are aware of that Qext alone is not sufficient to quantify contribution of large and small raindrops to total attenuation. However, our intention was to emphasize

different sensitivity to raindrops for frequencies used by E-band CMLs (73 and 83 GHz) and frequencies typically used in older CML networks (23 and 38 GHz), which can be demonstrated using extinction efficiency. For the sake of brevity, we have decided to remove the text explaining extinction-efficiency as well as figure 2, as they are not essential for further analyses. The statements that attenuation–rainfall model at E-band frequencies might be more sensitive to DSD are supported by the references to other studies.

C19) Line 143. I think this is an important part and would be great to have it formulated mathematically as it has been done for RR attenuation. The combination of sections 2.3 and 2.4 models might result in better estimates of RR due to the consistent adjustment of WAA.

A19: Thank you for this suggestion. However, formulating mathematically WAA is too complex problem and out of the scope of this paper. Instead, we have added at this place text referring to two recent studies numerically simulating WAA: "WAA can be modeled using EM full-wave simulators (Mancini et al., 2019; Moroder et al., 2020) *solving numerically Maxwells's equations, nevertheless, such simulations are computationally demanding and require characterizing distribution of water (e.g. thin film, droplets, rivulets) and its volume on antenna radomes."*

C20) Section 3.1 and 3.2 are confusing. Wouldn't be better presenting the Duebendorf and the Prague datasets altogether? I think it makes much more sense to say what is each dataset scope, instrumentation, measuring periods, and available data instead of having these three pieces of information scattered around into two sections and three subsections.
The model to discriminate between stratiform and convective precipitation is a method well suited for the Duebendorf dataset part.
Dry and wet weather discrimination fits well the Prague dataset processing, also WAA estimation belongs to this section.

A20: Agreed. We have merged sections 3.1 and 3.2 of the original MS.

C21) Line 222 - Would be better to be quantitative here. What do the authors mean with mean MSL pressure? Could be an international standard atmosphere, Mid-latitude, mean MSL pressure in Prague, or others. Just reporting the number is sufficient.

A21: Agreed. It is 1013 hPa.

C22) Line 305 It is either "An are rainfall induced attenuations" or "A is rainfall induced attenuation"

A22: Thank you, we have corrected this typo.

C23) Figure 6 - The correlation coefficient (CC is of little use to evaluate the discrepancies between observed and simulated attenuation. What a high CC value tells is that if one quantity is increasing or decreasing, the other is doing the same. It does not provide information on constant biases and drifts of the two quantities.
I am not really sure of what is the information that I can get from the linear fits to the data (not discussed in the text).
In such scatterplots, it is usually more interesting to evaluate the deviations of the data from the 1:1 to analyze systematic biases and trends. The discussion up the correlation coefficients at lines 355-359 doesn't seem relevant to me, it also makes December look like the worst-

case (smallest CC) while from a visual inspection it is probably the moth giving the best agreement between observed and simulated attenuation.
It seems that the theoretical attenuation is limited to values smaller than 3 dB while the observed ones go up to 6 dB, I wonder what could cause such discrepancies (uncertainties in the humidity measurements or in the evaluation of the measured gas attenuation perhaps). Comparing the distributions of attenuation values might be informative.

A23: Indeed, the correlation does not provide information about constant biases and drifts. We have, therefore, decided to complete scatter plots (Figure 8 in the revised MS) with RMSE and mean deviation between theoretical and observed attenuation and comment on these results also in the text (lines 417-420 of the revised MS). The linear fits were removed and 1:1 lines in the color of grid lines are now shown in the scatterplots.

The possible causes of discrepancies between theoretical and observed attenuation are discussed in the Discussion section (lines 536-546 of the revised MS). The highest discrepancies occur during longer dry weather periods, mostly during nights and might be related to multipath propagation, or condensation of water on antennas causing WAA. Such high discrepancies are unlikely to be caused by uncertainties in humidity observations. Temperature during these events do not exceed 10° C and water vapor densities should be below 10 g m^{-3}, causing at the long CML maximal theoretical gaseous attenuation not exceeding 0.45 dB/km. Moreover, humidity and temperature is measured independently at two sites and we did not observe differences which could explain such high deviations in observed attenuation.

C24) Lines 426-430 - It is less than surprising that the results of the ITU and the stratiform-DSD-derived k-R model give similar results given the fact that for low-intensity precipitation they are almost indistinguishable (Fig. 8)

A24: There are actually discrepancies between these two models also for low intensities, which can be seen in detailed view shown on the figure R3 below. The top panels show all four models and the bottom panels show difference between k-R model derived for stratiform rainfalls and ITU based model. The ITU model underestimates rainfalls compared to stratiform model for rainfall intensities up to about 2 mm/h. The highest underestimation compared to stratiform model (by 0.2 and 0.16 mm/h for 73.5 resp. 83.5 GHz frequencies) is reached for specific attenuation around 1.1 dB/km (Fig. R3, bottom). For stratiform rainfalls, this attenuation corresponds to rainfall intensity approx. 1.3 mm/h and 1.0 mm/h for 73.5 resp. 83.5 GHz frequency.

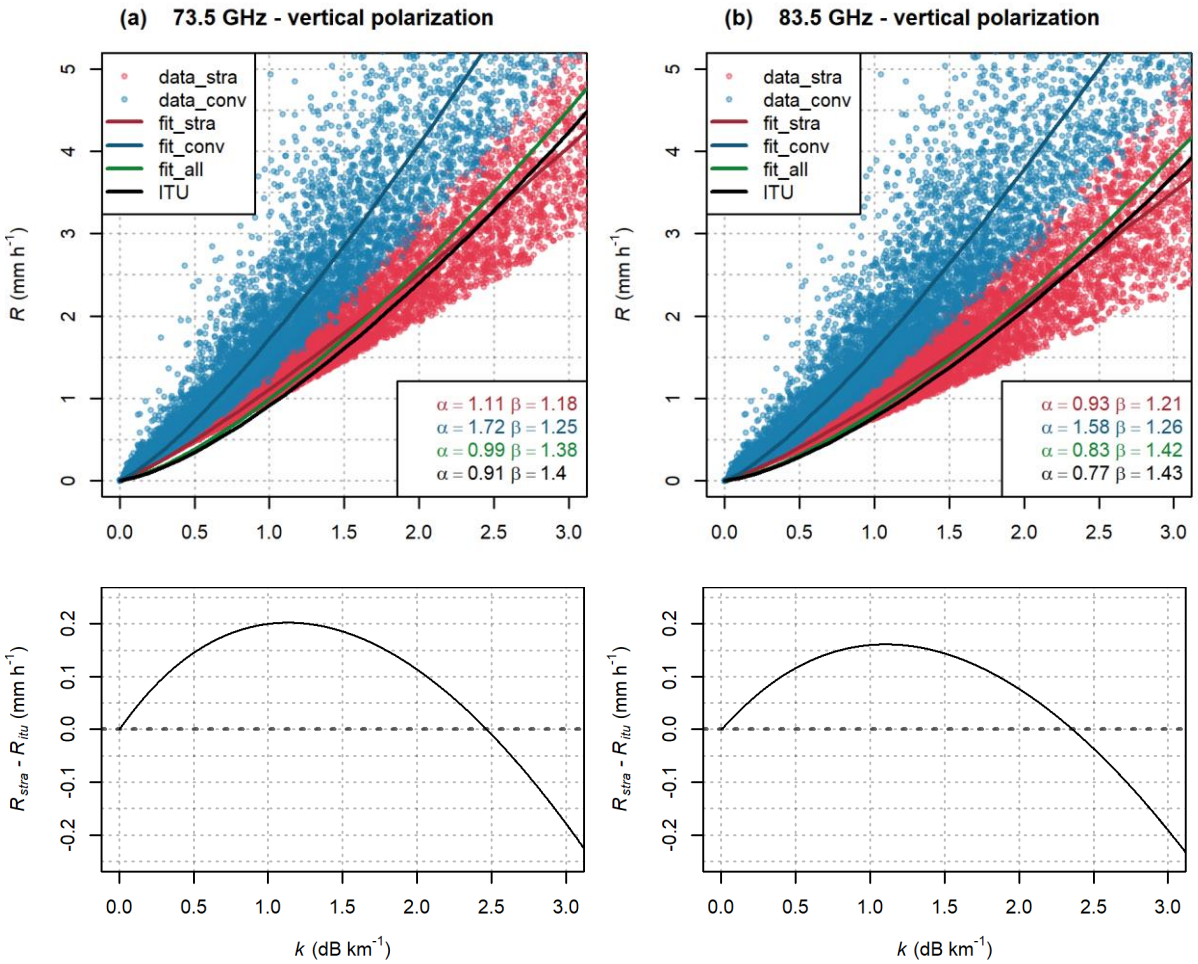

Figure R3: Difference between the k-R model derived for stratiform rainfall and the ITU-based k-R model.

The analysis estimating systematic and random errors of k-R models due to variable DSD was included into section 3.3 (lines 287-298). We have also added into Figure 8 (in the revised MS Figure 3) two insets with detail of low specific attenuations. The analysis of uncertainties provides in our view better insight than the table 4 presenting in the original MS k-R model discrepancies in terms of RMSE. We have, therefore, decided to remove this table from the revised MS. This resulted also in small changes in the Discussion section (lines 492-496 of the revised MS), where random and systematic errors are now discussed instead of RMSE.

C25) Line 537 - It is indeed surprising that the rainfall estimation performance turns out so good. The reason is that as Fig. 8 demonstrates there is already at low intensity quite a huge spread of points derived from the DSD data which should translate in a high uncertainty of the k-R model. Moreover, even a perfect k-R model is very sensitive to the uncertainties in the estimated attenuation. The comparison of panels a and b of Fig 11 show qualitatively how the distance between antennas influences the uncertainty in the measured k, but I would like to see that quantity assessed and the influence on the retrieved RR quantified.
Especially by looking at the 70GHz panels in Fig 11b it is possible to see the points of the scatterplot lining up. This probably indicates that the uncertainty in the measurements of k are specific to each receiving station. The separation into shorter and longer CML helps the

qualitative assessment, but again the authors miss the opportunity to evaluate the uncertainty of the k measurement as a function of the distance between the stations.

A25: We have separated deviation of CML QPEs into systematic and random component and related them to rainfall intensity (Fig. 10 of the revised MS). These deviations are then compared to expected systematic and random deviations i) due to deficits of the constant WAA model and, ii) due to DSD-related deficits of the ITU-based model. The evaluation of WAA considers explicitly length of CMLs. The results indicate, that DSD related errors are relatively small for short CMLs and for light rainfall intensities. On the other hand, the effect of DSD is significant for the long CML and can explain large part of random and systematic deviations in observed CML QPEs.
WAA seems to be crucial source of systematic error for shorter CMLs, which correspond to our results. The evaluation of uncertainties enabled us interpreting in detail, how CML path length influence its accuracy (lines 451 -453): "In general, sensitivity to rainfall, which is proportional to a CML path length, seems to be crucial characteristic influencing accuracy of CMLs when observing light rainfalls under 2 mm h^{-1}*. For heavier rainfalls, other characteristic than path length influence the uncertainties of CMLs more significantly." We hypothesize that differences in WAA patterns are due to different aging of coating, nevertheless, the coating was not directly investigated in this study.*
Furthermore, quantification of WAA (section 3.4 in the revised MS) is now extended by evaluation of systematic and random errors related to the modeling WAA as a constant offset.

OTHER CHANGES NOT REPORTED IN THE ANSWERS TO THE COMMENTS:

Rev 26: Section 2.2 describing gaseous attenuation and its quantification explains briefly in the revised MS also principle behind water vapor retrieval and refers to two studies using CMLs for this purpose.

Rev 27: Coordinates of CMLs in the section 3.1 had to be removed due to concerns of mobile network operator. We, nevertheless, believe that Figure 2 provides sufficient information on the case study layout.

Rev 28: Discussion section was restructured (reordered) to reflect updated structure of Method and Result section.

Rev 29: Differences between rain gauges quantified in terms of standard deviation are reported at lines 508-510, where assumptions on rainfall spatial uniformity during quantification of WAA are discussed.

REFERENCES (ANSWERS):

Berne, A. and Uijlenhoet, R.: Path-averaged rainfall estimation using microwave links: Uncertainty due to spatial rainfall variability, Geophys. Res. Lett., 34(7), L07403, doi:10.1029/2007GL029409, 2007.

Jaffrain, J. and Berne, A.: Quantification of the Small-Scale Spatial Structure of the Raindrop Size Distribution from a Network of Disdrometers, J. Appl. Meteor. Climatol., 51(5), 941–953, doi:10.1175/JAMC-D-11-0136.1, 2012.

Mancini, A., Lebrón, R. M. and Salazar, J. L.: The Impact of a Wet S-Band Radome on Dual-Polarized Phased-Array Radar System Performance, IEEE Transactions on Antennas and Propagation, 67(1), 207–220, doi:10.1109/TAP.2018.2876733, 2019.

Meshesha, D. T., Tsunekawa, A., Tsubo, M., Haregeweyn, N. and Adgo, E.: Drop size distribution and kinetic energy load of rainfall events in the highlands of the Central Rift Valley, Ethiopia, Hydrological Sciences Journal, 59(12), 2203–2215, doi:10.1080/02626667.2013.865030, 2014.

Moroder, C., Siart, U., Chwala, C. and Kunstmann, H.: Modeling of Wet Antenna Attenuation for Precipitation Estimation From Microwave Links, IEEE Geoscience and Remote Sensing Letters, 17(3), 386–390, doi:10.1109/LGRS.2019.2922768, 2020.

Olsen, R., Rogers, D. and Hodge, D.: The aRbrelation in the calculation of rain attenuation, IEEE Transactions on Antennas and Propagation, 26(2), 318–329, doi:10.1109/TAP.1978.1141845, 1978.

Overeem, A., Leijnse, H. and Uijlenhoet, R.: Measuring urban rainfall using microwave links from commercial cellular communication networks, Water Resources Research, 47(12), doi:10.1029/2010WR010350, 2011.

Schleiss, M. and Berne, A.: Identification of Dry and Rainy Periods Using Telecommunication Microwave Links, IEEE Geoscience and Remote Sensing Letters, 7(3), 611–615, doi:10.1109/LGRS.2010.2043052, 2010.

Schleiss, M., Rieckermann, J. and Berne, A.: Quantification and Modeling of Wet-Antenna Attenuation for Commercial Microwave Links, IEEE Geoscience and Remote Sensing Letters, 10(5), 1195–1199, doi:10.1109/LGRS.2012.2236074, 2013.

SOME REFERENCES (COMMENTS):

Battaglia, A., M. O. Ajewole, and C. Simmer, 2006: Evaluation of Radar Multiple-Scattering Effects from a GPM Perspective. Part I: Model Description and Validation. J. Appl. Meteor. Climatol., 45, 1634–1647, https://doi.org/10.1175/JAM2424.1.

Berne, A. and Uijlenhoet, R.: Path-averaged rainfall estimation using microwave links: Uncertainty due to spatial rainfall
variability, Geophys. Res. Lett., 34(7), L07403, doi:10.1029/2007GL029409, 2007.

Fujiwara, M.: Raindrop-size Distribution from Individual Storms, J. Atmos. Sci., 22(5), 585–591, doi:10.1175/1520-
0469(1965)022<0585:RSDFIS>2.0.CO;2, 1965

Illingworth, A. J., and T. M. Blackman, 2002: The Need to Represent Raindrop Size Spectra as Normalized Gamma Distributions for the Interpretation of Polarization Radar Observations. J. Appl. Meteor., 41, 286–297, https://doi.org/10.1175/1520-0450(2002)041<0286:TNTRRS>2.0.CO;2.

Ulbrich, C. W.1983. Natural variations in the analytical form of the raindrop size distribution.J. Climate Appl. Meteor.22:1764–1775

Atmospheric observations with E-band microwave links – challenges and opportunities

Martin Fencl[1], Michal Dohnal[1], Pavel Valtr[2], Martin Grabner[3], Vojtěch Bareš[1]

[1]Department of Hydraulics and Hydrology, Czech Technical University in Prague, Prague 6, 166 29, Czech Republic
[2]Department of Electromagnetic Field, Czech Technical University in Prague, Prague 6, 166 29, Czech Republic
[3]Department of Frequency Engineering, Czech Metrology Institute, Brno, 638 00, Czech Republic

Correspondence to: Martin Fencl (martin.fencl@cvut.cz)

Abstract. Opportunistic sensing of rainfall and water vapor using commercial microwave links operated within cellular networks was conceived more than a decade ago. It has since been further investigated in numerous studies, predominantly concentrating on the frequency region of 15–40 GHz. This manuscript provides the first evaluation of rainfall and water vapor sensing with microwave links operating at an E-band (specifically, 71–76 GHz and 81–86 GHz), which are increasingly updating, and frequently replacing, older communication infrastructure. Attenuation-rainfall relations are investigated theoretically on drop size distribution data. Furthermore, quantitative rainfall estimates from six microwave links, operated within cellular backhaul, are compared with observed rainfall intensities. Finally, the capability to detect water vapor is demonstrated on the longest microwave link measuring 4.86 km in path length. The results show that E-band microwave links are markedly more sensitive to rainfall than devices operating in the 15–40 GHz range and ~~are thus able to~~can observe even light rainfalls, a feat practically impossible to achieve previously. The E-band links are, however, substantially more affected by errors related to variable drop size distribution. Water vapor retrieval might be possible from long E-band microwave links~~,~~; nevertheless, the efficient separation of gaseous attenuation from other signal losses will be challenging in practice.

1 Introduction

Electromagnetic (EM) waves in the microwave region are attenuated by water vapor, oxygen, fog, or raindrops. Measurements of microwave attenuation at different frequency bands thus represent an invaluable source of information regarding the atmosphere. Passive and active microwave systems have become an integral part of Earth~~–~~-observing satellites, terrestrial remote sensing systems, and complete remote sensing methods in other spectral regions (Woodhouse, 2017). The microwave region is, however, also increasingly utilized in communication systems allowing for new possibilities to observe atmosphere with unintentional (opportunistic) sensing. Commercial microwave links (CMLs) are an excellent example of a communication system capable of providing close-to-ground observations of the atmosphere. CMLs are point-to-point line-of-sight radio connections widely used in mobile phone backhaul for connecting hops of different lengths, typically ranging from tens of meters to several kilometers. ~~There were about~~About 4 million CMLs were operated worldwide within cellular backhaul in

2016 (Ericsson, 2016) and about 5 million in 2018 (Ericsson, 2018). Most of these CMLs ~~operate~~are operated at frequencies between 15 and 40 GHz (Ericsson, 2016, 2018), where raindrops and, to a lesser extent, water vapor represent a significant source of attenuation (Atlas and Ulbrich, 1977; Liebe et al., 1993). Information on the attenuation of any CML within countrywide networks is virtually accessible in real-time with a delay of several seconds from a remote location, typically a network operation center (Chwala et al., 2016) creating an appealing opportunistic sensing system capable of providing close-to-ground observations of rainfall intensity (Leijnse et al., 2007; Messer et al., 2006) and water vapor density (David et al., 2009).

CML rainfall retrieval methods developed over the last decade have been predominantly designed and tested for frequency bands between 15 and 40 GHz (Chwala and Kunstmann, 2019). Attenuation caused by raindrops is, in this frequency region, almost linearly related to rainfall intensity and does not strongly depend on drop size distribution (DSD) (Berne and Uijlenhoet, 2007). Water vapor retrieval has been proposed for CMLs operating around 22 GHz (David et al., 2009), where there is a resonance line of water vapor. Increasing demands on data transfers force operators to utilize higher frequency spectra and a new generation of E-band CMLs, operating at the 71 - 86 GHz frequency band, is gradually modernizing cellular backhaul networks, especially in cities, where they often replace older devices. The share of E-band CMLs in mobile phone backhaul has already reached 20 %, *e.g.*, in Poland and the Czech Republic, and it is expected to grow in other countries as E-band CMLs are considered an essential part of new 5G networks (Ericsson, 2019).

E-band CMLs should be, according to recommendations for designing CMLs (ITU-R, 2005), more sensitive to rainfall, nevertheless, the relation between rainfall intensity and attenuation is not linear. Furthermore, E-band radio waves have two to four time's shorter wave lengths and the extinction efficiency ~~(resonance peak)~~ is highest for smaller raindrops. The attenuation-rainfall relation is, thus, more sensitive to drop size distribution, which has been already demonstrated in several propagation experiments, *e.g.*, ~~by Hansryd et al., (2010) or Luini et al. (2018)~~by Hansryd et al., (2010) or Luini et al. (2018). Radiowave propagation at an E-band is also more sensitive to water vapor, which poses a challenge when separating rainfall-induced attenuation from other sources of attenuation. On the other hand, the sensitivity to water vapor might also enable its detection or even monitoring.

This manuscript provides the first evaluation of E-band CMLs as rainfall and water vapor sensors. The capabilities of E-band CMLs for weather monitoring are theoretically evaluated and demonstrated on attenuation data retrieved between August and December 2018 from a six E-band CML operated within cellular backhaul of a commercial provider in Prague (T-Mobile, CZ). The ultimate goal of this investigation is to provide an overview of the challenges and opportunities related to atmospheric observations with E-band CMLs. Section 2 of the manuscript summarizes, based upon previous works, the principles behind retrieving atmospheric variables from CML observations, Section 3 describes the methodology and datasets used in this manuscript for the assessment of E-band CMLs, ~~Section 4 presents the results of the case study~~in addition, analysis estimating wet antenna attenuation and ~~evaluates~~analysis evaluating the effect of DSD on the attenuation-rainfall relation~~.~~ are presented. Section 4 presents the results of the case study. The results are further interpreted and discussed in Section 5, followed by the conclusions ~~which are~~ presented in Section 6.

2 Retrieving atmospheric variables from CMLs – theoretical background

2.1 Components of total observed loss

Standard CMLs are monitored for transmitted *tx* (dBm) and received *rx* (dBm) signal power and the difference between *tx* and *rx* is the total observed loss L_t (dB~~)~~), which can be separated into several components:

$$L_t = ~~L_{bf}~~ tx - rx = L_{bf} + L_m + L_{tc} + L_{rc} - G_t - G_r, \quad (1)$$

where L_{bf} (dB) is free space loss, L_m (dB) are losses in the medium, L_{tc} (dB) and L_{rc} (dB) are losses at the transmitting and receiving antennas, and G_t (dB) and G_r (dB) are antenna directive gains (Internationale Fernmelde-Union, 2009). Free space loss L_{bf} is uniquely defined by the distance d (m) between the transmitter and receiver, and by wavelength λ (m):

$$L_{bf} = 20\left(\frac{4\pi d}{\lambda}\right) \quad (2)$$

The sum of antenna losses and gains is given by their hardware ~~and~~. It includes interference with the environment close to antennas as antenna loss can change, *e.g.*, due to the wetness of antenna radomes. The propagation mechanisms influencing loss in the medium L_m consist of attenuation due to atmospheric gases, including water vapor, which is usually not exceeding 1.5 dB km^{-1} (section 2.2), attenuation due to precipitation, which can reach several tens of dB km^{-1} (section 2.3), attenuation due to obstacles in the wave path, and diffraction losses causing bending of the direct wave towards the ground. Total loss can also be influenced by so-called multipath interference occurring due to the constructive or destructive phase summation of the signal at the receiving antenna during the atmospheric multipath propagation conditions (Valtr et al., 2011). Precise separation and quantification of different components of total loss requires detailed description of atmospheric conditions along a CML path as well as conditions affecting hardware of transmitting and receiving stations. The specific path-attenuation due to raindrops or due to water vapor k (dB km^{-1}) is thus usually separated from other sources of attenuation using data-driven approach:

~~The separation of attenuation due to rainfall and due to water vapor from other sources of attenuation, is possible to some extent, but, firstly, dry and wet weather periods need to be identified~~ $k = max\left(\frac{L_t - B - Aw}{l}, 0\right)$ (3)

where l (km) CML path length, B (dB) is background attenuation, so-called baseline, and Aw (dB) wet antenna attenuation (WAA) caused by antenna radome wetting during rainfall or dew events. Baseline is most commonly estimated from attenuation levels during periods without rain and dew on antennas (Overeem et al., 2011; Schleiss and Berne, 2010). ~~Attenuation during dry weather is assumed to be a baseline, and the difference between dry and wet weather attenuation is then attributed to rainfall. Fluctuations in the baseline during dry weather can be attributed to water vapor, nevertheless, they can also be caused by temperature changes, hardware instability, etc.~~

~~The correct~~WAA estimation ~~of raindrop path attenuation and water vapor attenuation also requires the separation of additional attenuation caused by antenna radome wetting, so-called wet antenna attenuation (WAA) (~~is discussed in more detail in section

2.4~~). This~~ . The accurate quantification of WAA is especially important for shorter CMLs ~~which are~~ attenuated by raindrops along the short path and the relative importance of WAA contribution is significant.

We further refer to the periods with and without rain and dew occurrence as wet resp. dry weather. The term loss is used when referring to reduction in power density of EM wave in dB. In contrast, the term attenuation mostly refers to specific attenuation (dB km^{-1}) apart from WAA where it means loss (dB). We, nevertheless, stick to the term WAA as it is already established in the literature.

2.2 Attenuation by atmospheric gasses

Attenuation by atmospheric gasses is caused predominantly by the interaction of an EM wave with molecules of water and oxygen. The evaluation of gas attenuation, as described in ~~ITU-R (2019)~~ITU-R (2019) and originally in Liebe et al. (1993), is based on the concept of the complex refractive index. In a medium with complex refractive index n, the intensity of EM wave I (W m^{-2}) is attenuated at distance x (m) as:

$$I(x) = I(0)\, exp(-2\kappa\, Im(n)\, x), \qquad (3\underline{4})$$

where κ = ~~2π~~$2\ 10^9\ \pi\ f / c$ (m) is a vacuum wave number, f (GHz) the EM wave frequency, c (m s^{-1}) speed of light, and $Im(n)$ denotes the imaginary part of n. After introducing complex refractivity $N = (n\text{-}1)10^6$, the specific attenuation k (dB km^{-1}) is obtained as:

$$k = 10\, log_{10}\left(\frac{I(0)}{I(1)}\right) = 0.1819\, f\, Im(N), \qquad (4\underline{5})$$

~~where f (GHz) is~~with the EM wave frequency f expressed in GHz.

~~The~~ In (Eq. 5), the attenuation due to water vapor is ~~in here~~ defined as the difference between wet-air and dry-air attenuation under the same moist-air pressure and temperature. Thus ~~also~~, the effect of water vapor on dry-air attenuation is considered (ITU-R, 2019)~~: First, dry-air pressure decreases during humid conditions (under the assumption of constant moist-air pressure) and second, partial water-pressure affects the rate of collisions between the molecules (pressure broadening). Figure 1 shows specific attenuation by water vapor and dry air. Attenuation due to water vapor increases as the frequency increases, with the exception of the peak around 22 GHz and the depression around 60 GHz (Fig. 1a). The sensitivity of water-vapor attenuation to temperature and air pressure monotonically increases as the frequency increases. The temperature and pressure also influence dry-air attenuation, especially at frequencies around 60 GHz (Fig. 1b).~~

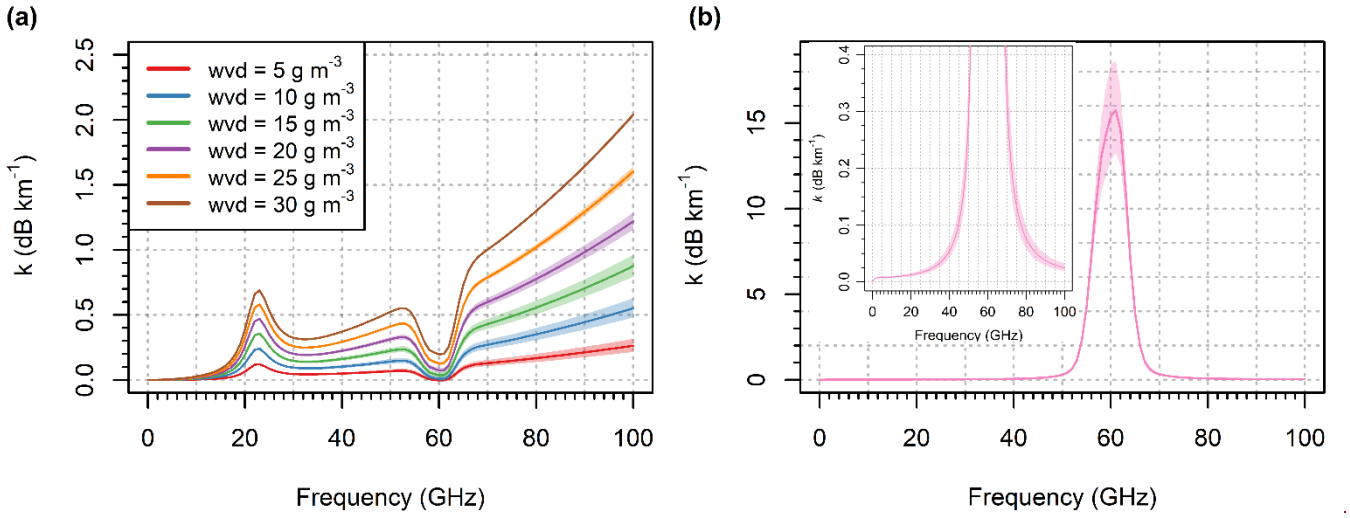

: First, dry-air pressure decreases during humid conditions (under the assumption of constant moist-air pressure), and second, partial water pressure affects the rate of collisions between the molecules (pressure broadening). Figure 1 shows specific attenuation by water vapor and dry air. Attenuation due to water vapor monotonically increases as the water vapor density increases. Water vapor density can be thus uniquely determined from gaseous attenuation when temperature and air pressure is known. David et al., (2009) suggested that CMLs operating around 22 GHz might be sufficiently sensitive to gaseous attenuation enabling estimation of water vapor density. Recently, daily water vapor estimates from multiple CMLs operating around 22 GHz were evaluated (David et al., 2019), nonetheless, water vapor retrieval from E-band CMLs has not been reported yet. Water vapor attenuation at E-band is about two times higher than around 22 GHz, however, it is also significantly more sensitive to temperature and to lesser extent to air pressure (Fig. 1a). The temperature and pressure also influence dry-air attenuation, especially at frequencies closer to 60 GHz (Fig. 1b).

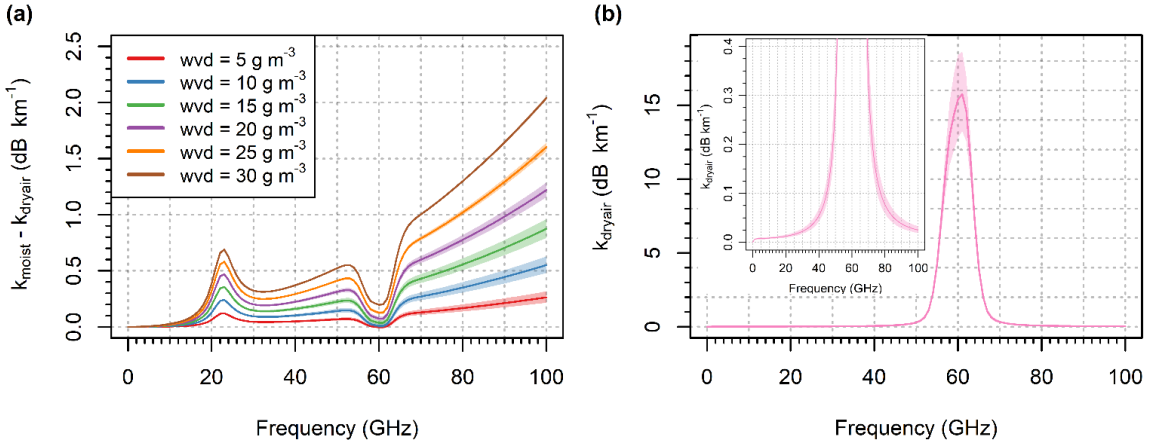

Figure 1: (a) Attenuation of EM by water vapor for frequencies 0 to 100 GHz. The relation is shown for different water vapor densities (wvd) for temperatures -10° to +30° C and pressure 1000 to 1030 hPa (colored bands). (b) Dry ~~-~~air attenuation of EM for temperatures -10° to +30° C and pressure 1000 to 1030 hPa (total spread represented by colored bands), inset: a detailed view of the lower attenuations.

2.3 Relation between raindrop path attenuation and rainfall intensity

Attenuation of a direct EM wave due to raindrops can be precisely calculated using the scattering theory. Attenuation caused by a single raindrop is determined by the wavelength, refractive index of water, and shape parameters of the raindrop~~.~~ and its orientation. The extinction cross section C_{ext}, (cm^2~~)~~), which can be calculated using the T-matrix method (Mishchenko and Travis, 1998), characterizes the scattering and absorption properties of each raindrop for a given frequency and polarization. The ~~number of drops~~total drop density in the unit volume ~~per drop diameter interval $N(D)$~~N_t (m^{-3} ~~mm^{-1}~~) is relatively small for natural rainfalls. Therefore, ~~the contribution of scattered secondary EM waves radiated from particles to the incident field of the other particles is negligible~~multiple scattering effects can be neglected. The specific raindrop path attenuation k (dB km^{-1}) can be thus considered as a sum of attenuations caused by single raindrops ~~of diameter D (mm)~~ and can be expressed in integral form:

$$k(f) = \text{~~}4.343 \times 10^{3} \int_{D_{min}}^{D_{max}} C_{ext}\,(D,f) N(D)\, dD\text{~~}\; 0.4343 \int_{D_{min}}^{D_{max}} C_{ext}\,(D,f) N(D)\, dD, \quad (5\text{~~}6)$$

where D (mm) denotes the equivolumetric spherical drop diameter, $N(D)$ (m^{-3} mm^{-1}) is number of drops in unit volume per drop diameter interval. The $N(D)$ also determines rainfall intensity R (mm h^{-1}):

$$R = 0.6\,\pi\,10^{-3} \int_{D_{min}}^{D_{max}} v(D)\, D^3 N(D)\, dD, \quad (6\text{~~}7)$$

~~where $v(D)$ (m s^{-1}) is the terminal velocity of raindrops given by their diameters. As both specific attenuation and rainfall intensity are moments of drop size distribution (DSD), the relation between attenuation and rainfall intensity can be approximated by a power law:~~

where $v(D)$ (m s^{-1}) is the terminal velocity of raindrops given by their diameters. The relation between attenuation and rainfall intensity can be approximated by a power-law (Olsen et al., 1978):

$$k = a\,R^{b}\,, \quad (7\text{~~}8)$$

where a (mm^{-b} h^{b} dB km^{-1}) and b (-) are empirical parameters dependent on frequency, polarization, and DSD. When estimating rainfall from observed attenuation, Eq. (~~7~~8) can be reformulated to:

$$R = \alpha\,k^{\beta}\,, \quad (8\text{~~}9)$$

where α (mm h^{-1} dB$^{-\beta}$ km$^{\beta}$) = $a^{-1/b}$ and β (-) = b^{-1}.

The model (~~7~~8) resp. (~~8~~9) approximates the attenuation-rainfall relation well at frequencies around 30 GHz~~, nonetheless~~. Nonetheless, errors increase for both lower and higher frequencies due to variable DSD (Berne and Uijlenhoet, 2007). Berne and Uijlenhoet~~–~~ (2007), however, investigated sensitivity to DSD only for the frequency region of 5-50 GHz. A detailed evaluation of the attenuation-rainfall model for the E-band has not been reported, yet higher sensitivity of E-band CMLs to DSD has been demonstrated during several propagation experiments (Hansryd et al., 2010; Luini et al., 2018). ~~Furthermore, different sensitivities of E-band CMLs to DSD, compared to lower frequencies, is also obvious from their extinction efficiency:~~

~~$Q_{ext} = \frac{C_{ext}}{\sigma_{geo}}$, (9)~~

~~where C_{ext} (cm^2) and σ_{geo} (cm^2) are extinction resp. geometric cross sections of a raindrop. The extinction efficiency Q_{ext} of EM waves at the E-band is the highest for smaller raindrops (Fig. 2), which is characteristic for stratiform rainfalls, whereas larger raindrops characteristic for convective rainfalls (section 3.4) contribute relatively less to the total attenuation.~~

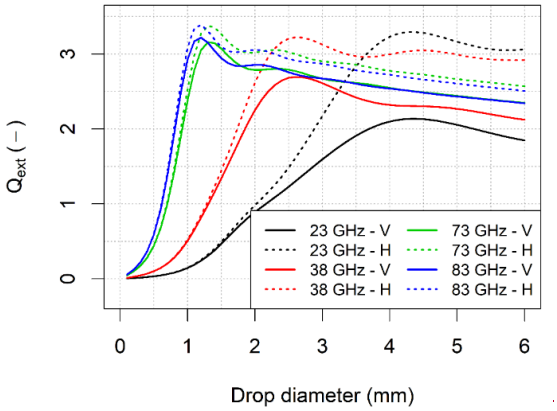

~~**Figure 2: Extinction efficiency of plane waves at different frequencies and polarizations (H – horizontal, V – vertical).**~~

2.4 Wet antenna attenuation

Wet antenna attenuation (WAA) is caused by a water layer forming on antenna radomes during rainfall events or dew occurrence. ~~Modeling WAA is challenging as the formation of water film on antennas is a complex process dependent on rainfall intensity, wind direction and velocity, or air and rain~~WAA can be modeled using EM full-wave simulators (Mancini et al., 2019; Moroder et al., 2020) solving numerically Maxwell's equations, nevertheless, such simulations are computationally demanding and require characterization of water distribution (*e.g.* thin film, droplets, rivulets) and its volume on antenna radomes. Formation of water film on antennas is, however, a complex process dependent on rainfall intensity, wind direction and velocity, or air and rain-water temperature, as well as on antenna radome hydrophobic properties. On the other hand, WAA represents a substantial part of total ~~attenuation~~loss (Fencl et al., 2019), especially by shorter CMLs, and its identification and separation from attenuation caused by raindrops along a CML path is crucial when obtaining reliable rainfall estimates.

Most of the models, ~~specifically~~ suggested explicitly for microwave link rainfall retrieval, are empirical and designed for lower frequencies (Minda and Nakamura, 2005; Overeem et al., 2011; Schleiss et al., 2013). However, the semi-empirical model suggested by Leijnse et al. (2008) enables WAA for an arbitrary frequency to be calculated. The Leijnse model assumes a layer of water with the constant thickness ~~which is~~ assumed to be power-law related to rainfall intensity. The parameters of this relation need to be optimized. According to the Leijnse model, WAA typical of E-band CML frequencies is about two times higher than ~~of~~ 38 GHz. Hong et al. (2017), however, showed on 72 and 84 GHz microwave links that WAA depends highly on specific hardware settings. An antenna without radome experienced WAA of about 7 dB during a spraying experiment with artificial rain. The antenna covered by a radome (~~which is~~ a typical setting of CMLs) experienced WAA of approx. 2 dB and WAA decreased further to only approx. 0.3 dB when a radome with hydrophobic coating was used. Similarly, low values of WAA at E-band CMLs have been reported by Ostrometzky et al. (2018), who observed WAAs of 0.86 ± 0.54 dB and 1.07 ± 0.75 dB at two 73 GHz CMLs. These values are significantly lower than previously observed WAA at lower frequencies (Fencl et al., 2018; Minda and Nakamura, 2005; Schleiss et al., 2013), although E-band CMLs should be, in theory, more sensitive to WAA (Leijnse et al., 2008).

3 Material and Methods

The E-band evaluation concentrates on i) separation of gaseous attenuation ~~and its relation to~~from total observed loss, which is a prerequisite for CML water vapor ~~density and air temperature~~retrieval, ii) the relation between raindrop attenuation and rainfall intensity, including the effect of DSD, and iii) ~~processing routines for separating different attenuation components.~~the influence of WAA on CML quantitative precipitation estimates (QPEs). The methodology combines numerical experiments using virtual attenuation time series simulated from weather observations with analyses of CML observations obtained during the dedicated case study. Datasets from two experimental sites are used for this purpose.

3.1 Experimental sites and ~~instrumentation~~datasets

Duebendorf data is used for analyzing sensitivity of attenuation-rainfall relation to drop size distribution. Drop size distribution is obtained from a PARSIVEL disdrometer (1st generation, manufactured by OTT). Drop counts and fall velocities are recorded over 30 s intervals. The data was collected during the CoMMon experiment in Duebendorf (CH~~) at site 2,~~), which is described, *e.g.*, in Wang et al. (2012). ~~We further refer to this dataset as~~ Duebendorf data~~.~~ span from March 2011 to April 2012.

~~The E-band evaluation case study is performed on six CMLs (Table 1) located in the south-east suburb of Prague (CZ).~~ The disdrometer data is quality-checked and suspicious records are excluded using filters described in Jaffrain and Berne (2010). Moreover, only records classified by the disdrometer as rainfall (at least from 90 %) are used for further analysis; hail events are excluded. In addition, particles larger than 5.5 mm are not considered to be raindrops and thus excluded from the analysis. The data which pass the quality check are aggregated to a 1-min temporal resolution using averaging.

Prague data is used for analyzing gaseous attenuation and evaluating rainfall retrieval from E-band CMLs. The CMLs (Table 1) are located in the south-east suburb of Prague (CZ). Five shorter CMLs are located in a residential area with a housing estate. The path of the long CML goes over an area with mostly agricultural land use (Fig. 2). The main node from which all CML paths originate is located on the roof of a 65-m-tall building; the end nodes are about 15 m to 30 m above ground. All the CMLs operate at an Ericsson MINILINK platform and were deployed to the site during 2016 and 2017. CMLs have a full-duplex configuration with two sub-links operating in one direction at 73–74 GHz and in the second direction at 83–84 GHz with a duplex separation of 10 GHz. Transmitted signal power *tx* and received signal power *rx* are collected with custom-made server-sided software which polls selected CMLs using SNMP protocol and stores records into a PostgreSQL database. The sampling time step is approx. 10 s. The resolution of a *tx* and *rx* reading is 0.1 dBm. All devices have automatic transmitted power control (ATPC), *i.e.*, transmitted power is automatically controlled to minimize fluctuations in *rx*. CML data acquisition is described in detail in the *Supplementary material*.

Tipping bucket rain gauges (MR3, METEOSERVIS v.o.s., catch area 500 cm^2, resolution 0.1 mm) have been deployed at four measuring sites. Two rain gauges are located at the end nodes of the long CML, one at ground level close to the CML path about 1.5 km from the main network node, and one about 2 km south-west from the main node. The rain gauges at sites 1 and 2 are equipped with temperature and air humidity sensors collecting observations in a 5-min time step. All four rain gauges have been regularly maintained (monthly~~Five shorter CMLs are located in a residential area with a housing estate. The path of the long CML goes over an area with mostly agricultural land use (Fig. 3). The main node from which all CML paths originate is located on the roof of a 65-m-tall building; the end nodes are about 15 m to 30 m above ground. All the CMLs operate at an Ericsson MINILINK platform and were deployed to the site during 2016 and 2017. CMLs have full-duplex configuration with two sub-links operating in one direction at 73–74 GHz and in the second direction at 83–84 GHz with a duplex separation of 10 GHz. Transmitted signal power *tx* and received signal power *rx* are collected with custom-made server-sided software which polls selected CMLs using SNMP protocol and stores records into a PostgreSQL database. The sampling time step is approx. 10 s. The resolution of a *tx* and *rx* reading is 0.1 dBm. All devices have automatic transmitted power control (ATPC), *i.e.*, transmitted power is automatically controlled to minimize fluctuations in *rx*. CML data acquisition is described in detail in the *Supplementary material*.~~

~~Tipping bucket rain gauges (MR3, METEOSERVIS v.o.s., catch area 500 cm^2, resolution 0.1 mm) have been deployed at four measuring sites. Two rain gauges are located at the end nodes of the long CML, one at ground level close to the CML path about 1.5 km from the main network node, and one about 2 km south-west from the main node. The rain gauges at sites 1 and 2 are equipped with temperature and air humidity sensors collecting observations in a 5-min time step.~~ ~~All four rain gauges have been regularly maintained (on a monthly basis~~) and are dynamically calibrated (Humphrey et al., 1997). We further refer to the case study dataset as Prague data (Fencl et al., 2020).

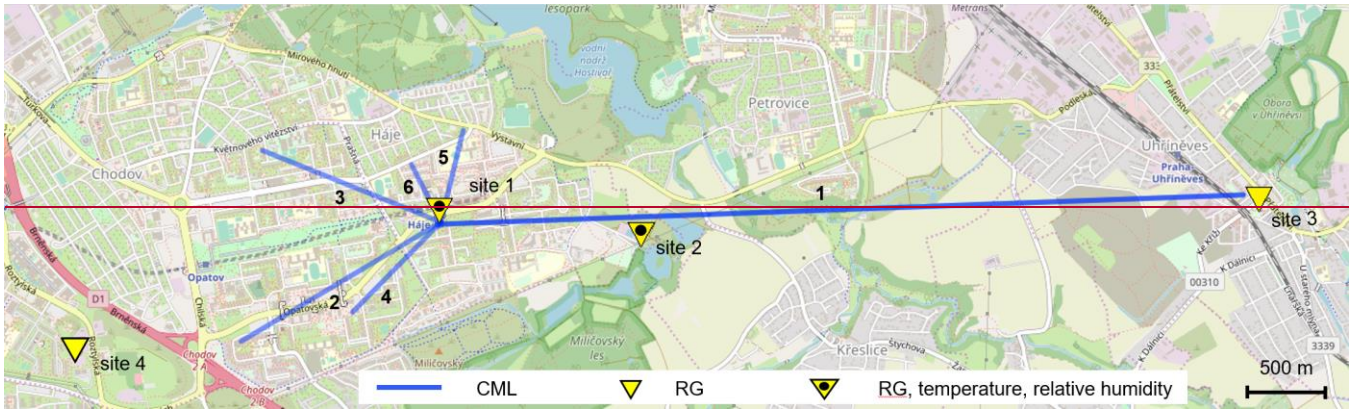

Figure 3: Case study area Prague-Haje, CZ. Two of the rain gauges are equipped with air humidity and temperature probes. ©OpenStreetMap contributors.

Table 1: CML characteristics in Prague-Haje, CZ. The suffixes A and B denote first, resp. second end node, and suffixes "a" and "b" the direction from A to B resp. B to A.

ID	LonA (deg)	LatA (deg)	LonB (deg)	LatB (deg)	Freq_a (GHz)	Freq_b (GHz)	Pol_a	Pol_b	Length (m)
1	14.5290	50.0301	14.5970	50.0317	73.5	83.5	V	V	4866
2	14.5291	50.0302	14.5122	50.0237	73.75	83.75	V	V	1409
3	14.5291	50.0302	14.5140	50.0341	72.75	82.75	V	V	1164
4	14.5291	50.0302	14.5216	50.0253	74.25	84.25	H	H	765
5	14.5310	50.0352	14.5291	50.0302	73	83	V	V	573
6	14.5291	50.0302	14.5266	50.0333	73.25	83.25	H	H	389

3.2 Experimental data

Experimental periods: Duebendorf data span from March 2011 to April 2012. Prague data span from 20th August to 16th December 2018. The rainfall observations are, due to technical problems available from 28th October to 16th December 2018.

Duebendorf data: The disdrometer data is quality checked and suspicious records are excluded using filters described in Jaffrain and Berne (2010). Moreover, only records classified by the disdrometer as rainfall (at least from 90 %) are used for further analysis; hail events are excluded. The data which pass the quality check are aggregated to a 1-min temporal resolution using averaging.

Prague data: Total loss is calculated for each CML as the difference between transmitted and received signal powers. The total loss data is aggregated using averaging to a 1-min temporal resolution.

Rain-gauge data are separated into rainfall events. An event is defined as a period with intervals between consecutive rain gauge tips shorter than one hour. The rainfall events with rainfall depth lower than 1 mm are excluded from the evaluation. Furthermore, events during which the temperature dropped below 2° C were also excluded from the evaluation to limit the performance assessment to liquid precipitation only. This results in a set of five events (see Table 2) representing, in terms of total depth, 81 % of all the precipitation during the experimental period. Rainfall data are aggregated by averaging to a 15-min temporal resolution to limit uncertainties due to rain gauge quantization and uncertainties related to uncaptured rainfall spatial variability. The 15-minute rainfall intensities are, for all four rain gauges, highly correlated (r = 0.88–0.96). The cumulative rainfall observed by the rain gauges is also in ~~very good~~excellent agreement and differs from the mean rainfall only by 1–3 %. The air temperature and relative humidity data (5-min temporal resolution) are not further processed. The correlation coefficient between temperature observations is 0.95 and between humidity observations 0.86. In general, observations on the ~~roof of the~~ 65-m-tall building (site 1) have slightly lower variability than close-to-ground observations (site 2). The discrepancies are especially pronounced during transient conditions in the morning. Prague data span from 20th August to 16th December 2018. The rainfall observations are, due to technical problems available from 28th October to 16th December 2018.

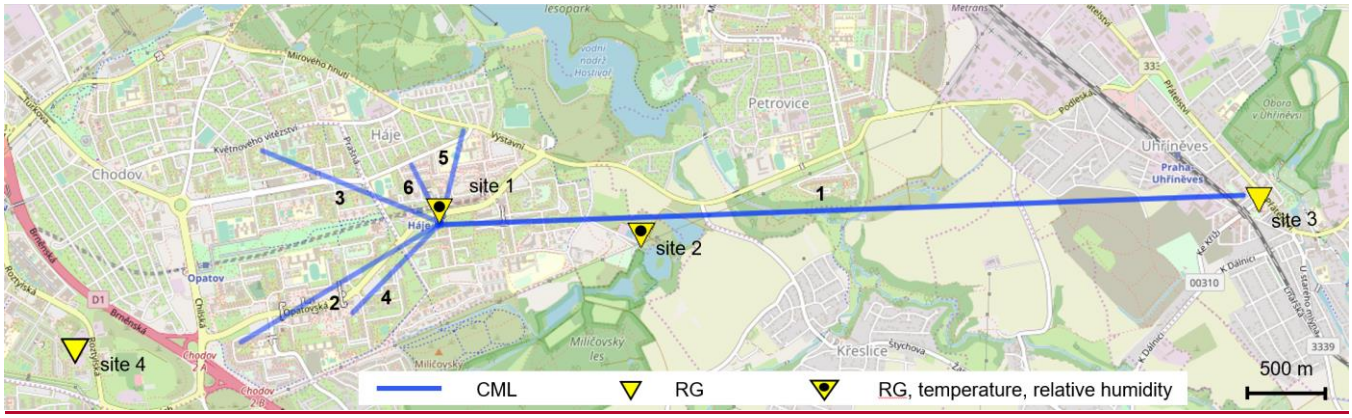

Figure 2: Case study area Prague-Haje, CZ. Two of the rain gauges are equipped with air humidity and temperature probes. ©OpenStreetMap contributors.

Table 1: CML characteristics in Prague-Haje, CZ. The suffixes "a" and "b" denote sub-links of a CML.

ID	Freq_a (GHz)	Freq_b (GHz)	Pol_a	Pol_b	Length (m)
1	73.5	83.5	V	V	4866
2	73.75	83.75	V	V	1409
3	72.75	82.75	V	V	1164
4	74.25	84.25	H	H	765
5	73	83	V	V	573
6	73.25	83.25	H	H	389

Table 2: Rainfall events used for the evaluation of CML rainfall retrieval

Event start	Duration (min)	Depth (mm)	R_{max} (mm h^{-1})
2018-10-28 01:10	1218	21.0	4.4
2018-11-02 19:14	500	5.1	2.5
2018-11-24 09:46	176	1.9	1.7
2018-12-03 05:00	158	1.8	2.6
2018-12-03 22:03	210	4.9	3.0

~~**3.3 Gaseous attenuation**~~

~~The effect of temperature and air humidity on total CML attenuation is estimated theoretically from observed air temperature and relative humidity (see section 2.2) and compared to the real CML data obtained during the case study from the long CML (ID 1). Atmospheric pressure was not measured and is assumed to be constant corresponding to average sea level pressure. Atmospheric pressure changes related to weather conditions have, however, an almost negligible effect on theoretical attenuation (ITU-R, 2019). The temperature and air humidity used in the analyses are averages from the observations at two locations along the CML path. Gaseous attenuation is estimated for the period from 20th August to 16th December 2018 and only considers dry weather, i.e., periods without rainfall and dew occurrences (events causing the tipping of at least one of the rain gauges). A safety window of 6 h was set before and after each event with an event considered to start with the first tip of any rain gauge and ending with the last tip.~~

~~**The theoretical attenuation derived from air temperature and relative humidity observations is then compared to the observed attenuation of the long CML. To enable a comparison, the observed attenuation is also aggregated to a 5-min time step corresponding to the time step of temperature and humidity observations, resp. theoretical attenuation. Furthermore, the constant baseline is subtracted from the observed attenuation**~~**3.2. CML data processing**

First, total loss is calculated for each CML as the difference between transmitted and received signal powers (Eq. 1). The total loss data is aggregated using averaging to a 1-min temporal resolution.

Quality check: All the time series of total losses are visually inspected to identify noticeable hardware related artifacts. In one case (CML 2), the sudden change in the baseline is manually corrected, as automated procedures used for attenuation processing are not designed to cope with this artifact. Hardware-related artifacts are in more detail presented in *Appendix B.*

Baseline identification for rainfall retrieval: Background attenuation, the so-called baseline, is needed to identify rainfall-induced attenuation (Eq. 3) and is estimated as a moving median with a centered window having a size of one week applied on time series of total losses averaged over 15-minute intervals. A one-week window size seems to be appropriate for the climate of the Czech Republic as it covers a period with more than half of the records belonging to dry weather. On the other

hand, it is sufficiently short to reliably capture long-term baseline drifts related to the instability of the CML hardware, or gaseous attenuation.~~,~~ Although dry-wet weather classification based solely on CML observations is not used for baseline identification in this study, it is included in *Appendix A* as it might be needed for future studies and applications (see Discussion section).

Baseline identification for evaluating gaseous attenuation: The constant baseline is set separately for each sub-link (73.5 GHz and 83.5 GHz), such as the median attenuation obtained after the baseline separation corresponds to the median theoretical attenuation~~.~~ (section 3.5). The median attenuation is calculated considering dry-weather periods only, *i.e.*, periods without rainfall and dew occurrences (events causing the tipping of at least one of the rain gauges). A safety window of 6 h was set before and after each event with an event considered to start with the first tip of any rain gauge and ending with the last tip.

~~.~~

~~The observed attenuation patterns are compared to the theoretical patterns calculated from temperature and air humidity observations assuming constant atmospheric pressure at sea level. The agreement between theoretical and observed attenuation is quantified in terms of correlations and the magnitude of their amplitudes. In addition, seasonal drift is demonstrated on time series smoothed by a moving average with a window size of one week.~~

~~**Table 3: Empirical parameters of convective and stratiform rainfall for DSD reconstruction as observed by Fujiwara (1965) and re-parameterized by Ulbrich (1983).**~~

~~Type~~	~~N_0 ($m^{-3}cm^{-1-\mu}$)~~	~~μ ( )~~	~~c (h^{δ})~~	~~δ ( )~~
~~Convective (thunderstorm)~~	~~$7.05 \cdot 10^4$~~	~~0.4~~	~~0.118~~	~~0.20~~
~~Widespread or stratiform~~	~~$1.96 \cdot 10^5$~~	~~0.18~~	~~0.082~~	~~0.21~~

~~Note: N_0 ($m^{-3}cm^{-1-\mu}$) and μ ( ) are parameters of semi-empirical gamma distribution function, c (h^{δ}) and δ ( ) are scaling parameters of this function.~~

Wet antenna attenuation: The WAA during rainfall is modeled as constant (Overeem et al., 2011) and is set to 2.7 resp. 2.3 dB for all 73– 74 GHz resp. 83–84 GHz sub-links. The magnitudes of WAA are estimated as the median of WAA values quantified during the analysis presented in section 3.4. The WAA magnitude of zero is considered during dry-weather periods.

3.43 Sensitivity of the k-R model to drop size distribution

The analysis of the k-R model (Eq. ~~8~~9) with respect to DSD is based on fitting Eq. (~~8~~9) on attenuation and rainfall intensities obtained from Eq. ~~(5) and~~ (6~~). c First, the sensitivity of the k-R model parameters (8) to the type of rainfall (stratiform vs. convective) is investigated on theoretical DSD and secondly on real DSD from the~~) resp. (7). The investigation is performed on PARSIVEL observations of DSD from Duebendorf dataset. The classification of rainfalls based on their mass-weighted diameter enables to optimize the k-R model separately for rainfall with different drop sizes.

Specific attenuations are calculated according to Eq. (6) for each DSD record. Extinction cross-sections entering Eq. (6) are calculated using T-Matrix model (Mishchenko and Travis 1998) implemented in Python (Leinonen, 2014). The calculation assumes temperature 10° C, canting angle 0°, drop shape being oblate spheroid, drop axial ratio according to Pruppacher and Beard (1970), and for drop smaller than 0.5 mm an own heuristic approximation of Pruppacher and Beard's formula is used. Specific attenuations are calculated for 73.5 and 83.5 GHz, vertical polarization, *i.e.*, frequencies of the sub-links belonging to the long CML in the Prague data. These frequencies are approximately in the middle of the frequency bands of 71–76 GHz and 81–86 GHz allocated for E-band fixed wireless services and, thus, representative for all E-band CMLs.

The rainfall records are classified into two groups according to the mass-weighted drop diameter D_m (mm), which is the ratio between the fourth and third DSD moments:

$$D_m = \frac{\int_{D_{min}}^{D_{max}} N(D) D^4 dD}{\int_{D_{min}}^{D_{max}} N(D) D^3 dD}$$

~~**Investigation of theoretical DSD:** The number of drops N with diameter D is modeled using the gamma distribution function scaled to rainfall intensity (Ulbrich, 1983). The parameters of gamma distribution for stratiform and convective rainfall are taken from Ulbrich (1983). The empirical parameters needed for the reconstruction of $N(D)$ for stratiform and convective rainfall are in Table 3. The distribution functions for two different rainfall intensities are shown in Fig. 4.~~

~~$N(D)$ is calculated for a sequence of reference rainfall intensities from 0 to 50 mm h^{-1} with an increment of 0.1 mm h^{-1} for both types of rainfalls. Specific attenuations corresponding to a given intensity and rainfall type are then calculated according to Eq. (5). Specific attenuations are calculated for 73.5 and 83.5 GHz, vertical polarization, *i.e.*, frequencies of the sub-links belonging to the long CML in the Prague data. These frequencies are approximately in the middle of the frequency bands of 71–76 GHz and 81–86 GHz allocated for E-band fixed wireless services and, thus, representative for all E-band CMLs.~~

~~The k-R model (Eq. 8) is fitted separately for each frequency and rainfall type by minimizing the sum of squared residuals between reference rainfall intensities (Eq. 6) and rainfall intensities estimated by the model using a specific attenuation obtained by Eq. (5).~~

~~**Investigation of Duebendorf DSD data:** The effect of DSD on the k-R power law approximation is further tested on DSD data (Duebendorf) and its influence on rainfall estimation accuracy is quantified. The procedure is analogous to the analysis of the theoretical DSD. However, rainfall intensities and specific attenuations are calculated from the observed DSD. The rainfall records are classified into two types according to the mass-weighted drop diameter D_m (mm), which is the ratio between the fourth and third DSD moments:~~

~~$$D_m = \frac{\int_{D_{min}}^{D_{max}} N(D) D^4 dD}{\int_{D_{min}}^{D_{max}} N(D) D^3 dD},$$~~ (10)

The mass-weighted diameter D_m is a common descriptor of the center of a probability density function $f(D)$ characterizing DSD. The mass-weighted diameter can be approximately related to the rainfall intensity by a power-law function:~~, thus the~~

$$\widehat{D_m} = \gamma R^{\delta},$$ (11)

where R (mm h^{-1}) is rainfall intensity and γ (mm mm$^{-\delta}$ h$^{\delta}$) and δ (-) are empirical parameters. The approximation (Eq. 11) is used to calculate classification threshold dependent on rainfall intensity. Parameters γ and δ are estimated by fitting Eq. (11) to D_m ~~based classification resembles the classification on convective and stratiform~~ as derived from PARSIVEL records using Eq. (10). Specifically, sum of squared residuals between D_m obtained from Eq. (10) and Eq. (11) is minimized. This results in parameters γ = 1.29 mm mm$^{-\delta}$ h$^{\delta}$ and δ = 0.16. D_m-based classification separates rainfalls by the size of their raindrops to two classes and roughly evaluates convective and stratiform nature of the precipitation in the Duebendorf dataset (Jaffrain and Berne, 2012). We further refer to those two classes as 'stratiform' and 'convective'. Records with *Dm* larger than or equal to capped *Dm* (Eq. 11) are classified as convective and time steps with *Dm* smaller than capped *Dm* are classified as stratiform.~~The mass-weighted diameter can be approximately related to the rainfall intensity by a power-law function:~~

~~$\widehat{D_m} = c\,R^d$, (11)~~

~~where R (mm h^{-1}~~The k-R model (Eq. 9) is fitted separately for each frequency and rainfall type by minimizing the sum of squared residuals between reference rainfall intensities (Eq. 7) and rainfall intensities estimated by the model using a specific attenuation obtained by Eq. (6). In addition, k-R model is also fitted for all the records together.

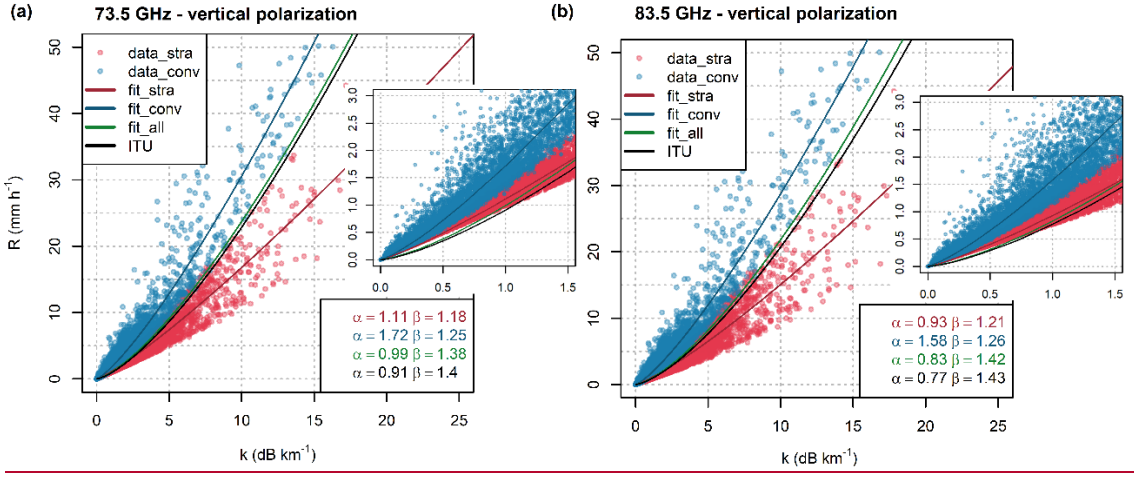

Figure 3: Relation between specific attenuation and rainfall derived from one year of DSD data for vertically polarized EM waves at (a) frequency 73.5 GHz, and (b) 83.5 GHz. Parameters of the k-R models (Eq. 9) are shown. Insets show in detail attenuation-rainfall relation and the k-R models for low specific attenuations and light rainfalls.

The relation between rainfall intensity and ~~c (h^{-d} mm$^{1/d}$) and d ( ) are empirical~~ theoretical attenuation obtained from Duebendorf PARSIVEL observations is shown, together with fitted k-R power-law curves, in Fig. 3. The k-R model with parameter optimized for all the records resembles closely the model with parameters according to ITU (ITU-R, 2005). The spread of rainfall intensity clearly grows with increasing attenuation. ~~. Such an approximation results in perfect fits~~The k-R model uncertainties, therefore, increase with increasing rainfall intensity. To evaluate expected accuracy and precision of k-R models, specific attenuation is subdivided into bins having size 0.1 dB km^{-1} in the range 0–4 dB km^{-1}, the bin size 0.5 dB km^{-1} is used for attenuation larger than 4 dB km^{-1}. Mean rainfall intensity and its standard deviation is calculated for each bin, first

using all the records and then separately for each rainfall class. Difference between the rainfall intensity obtained by k-R models (Eq. 9) and mean rainfall intensity can be then interpreted as a systematic deviation and standard deviation as a random error. We limit the evaluation to the attenuation range 0–7 dB km^{-1} to evaluate only bins with at least 10 records for stratiform ~~and~~or convective ~~rainfall types~~class.

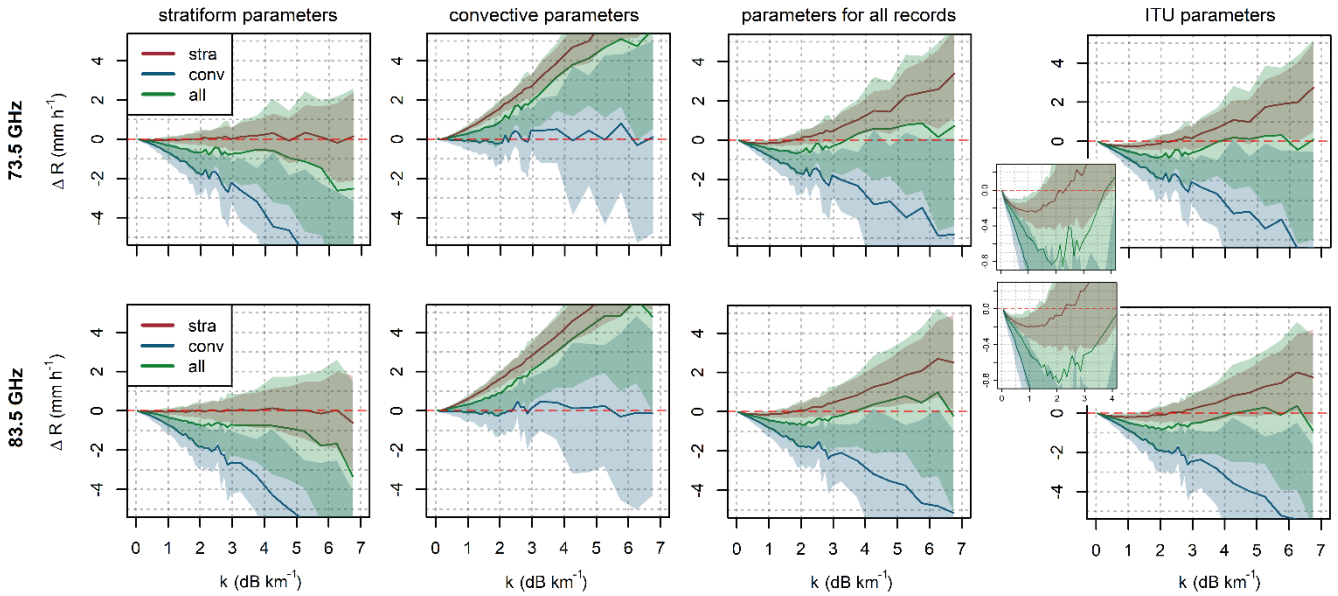

Figure 4: Systematic deviation of the k-R models with different parameters from mean rainfall intensities when applied to ~~theoretical DSD (Fig. 4b). The approximation (Eq. 11) is used to calculate threshold for classifying disdrometer records as convective or i)~~ stratiform~~. The threshold is dependent on rainfall intensity. Parameters *c* and *d*, ii) convective, and iii) all the rainfalls together. Random errors~~ are ~~estimated by fitting Eq. (11) to D_m as derived from real disdrometer data using Eq. (10).~~ depicted by bands corresponding to ± one standard deviation of rainfall intensities in a given bin. Insets show ITU model performance for specific attenuation range 0–4 dB km^{-1}.

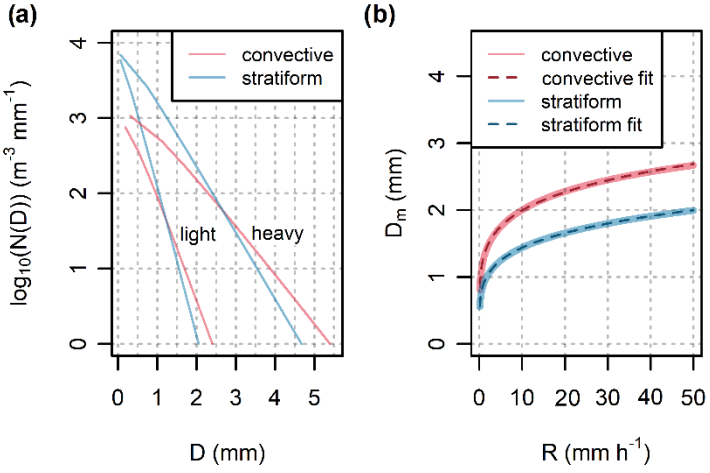

~~**Figure 4: (a) Theoretical DSD for light (1 mm h^{-1}) and heavy (50 mm h^{-1}) convective and stratiform rainfall, and (b) the power-law relation between mass weighted diameter D_m and rainfall intensity for the same rainfall types. Gamma distribution functions with parameters corresponding to storms reported by Fujiwara (1965) are used.**~~

Performance evaluation: The performance of k-R power-law approximation is evaluated by comparing rainfall intensities obtained directly from DSD (Eq. 6) to rainfall intensities estimated from the k-R model (Eq. 8). Virtual specific attenuations derived from DSD (Eq. 5) for two different frequencies are used as inputs to the k-R model. The performance is evaluated for three model settings: i) the k-R model with a single set of parameters obtained by fitting the model to the whole dataset, ii) the k-R model with two sets of parameters for periods with stratiform resp. convective rainfall obtained by fitting the model separately for these two rainfall types, iii) the k-R model with parameters from ITU recommendations (ITU-R, 2005).

The analysis is first evaluated for the theoretical DSD (theoretical PDFs describing drop size spectra) and secondly, in more detail, for DSD measured by a disdrometer. In the second analysis, the k-R model is evaluated in terms of root mean square error criterion (RMSE) for the whole dataset and then separately for light ($R \leq 4$ mm h^{-1}), moderate (4 mm h^{-1} $< R \leq$ 12 mm h^{-1}) and heavy ($R >$ 12 mm h^{-1}) rainfalls. The parameters of the k-R model obtained for Duebendorf data are verified on CML attenuation observations in Prague data.

3.5 CML rainfall retrieval

Rainfall retrieval is performed for each sub-link separately. First, total observed loss aggregated to a 1-min resolution is quality-checked. Second, total observed loss is aggregated to a 15-min temporal resolution and the baseline is identified and separated. Third, WAA is estimated and, finally, attenuation corrected for WAA is converted to rainfall intensity. Although dry-wet weather classification is not used for rainfall retrieval in this study, it is included in the *Appendix A* as it might be needed for future studies and applications (see Discussion section).

Quality check: All the time series of total losses are visually inspected to identify obvious hardware related artifacts. In one case (CML 2), the sudden change in the baseline is manually corrected, as automated procedures used for attenuation processing are not designed to cope with this artifact. Hardware-related artifacts are in more detail presented in *Appendix B*.

Baseline identification: Background attenuation, the so-called baseline, is needed to identify rainfall induced attenuation and is estimated as a moving median with a centered window having a size of one week applied on time series of total losses averaged over 15-minute intervals. A one-week window size seems to be appropriate for the climate of the Czech Republic as it covers a period with more than half of the records belonging to dry weather. On the other hand, it is sufficiently short to reliably capture long-term baseline drifts related to the instability of the CML hardware, or gaseous attenuation.

Figure 4 shows the expected systematic deviations and random errors of the k-R models (9) with different parameters. Bands representing random errors are constructed for each attenuation bin as ± one standard deviation of rainfall intensities. Systematic deviations and standard deviations are evaluated for each rainfall class separately and then for both classes together. All four k-R models have a similar patterns of deviation for 73.5 GHz and 83.5 GHz frequency. The k-R model with stratiform and convective parameters is almost unbiased when used for the corresponding class of rainfalls. Nevertheless, any misclassification of rainfall can result in large errors, especially during higher rainfall intensities. The k-R model with parameters for convective rainfall is affected by substantial random errors. For example, for specific attenuation 6 dB km^{-1}, which corresponds to mean convective rainfall approx. 8 mm h^{-1} and 9 mm h^{-1} for 73.5 resp. 83.5 GHz frequencies, the

standard deviation reaches 4 mm h^{-1}. The k-R models with ITU parameters and parameters optimized for all the rainfalls are with respect to systematic deviations more robust than 'stratiform' and 'convective' k-R models: Nevertheless, they are affected by larger random errors. Noteworthy, the k-R model with ITU parameters and parameters optimized for all the rainfalls systematically underestimate light rainfalls including those classified as stratiform (Fig. 4, insets).

3.4 Analysis of wet antenna attenuation

Wet antenna analysis is performed on attenuation~~:~~ data after baseline separation aggregated to 15 min. WAA during rainfall is estimated by comparing attenuations as observed by sub-links of different path lengths. WAA quantification assumes spatially uniform rainfall under which specific attenuations k_1, k_2, …, k_n (dB km^{-1}) of the sub-links 1, 2, …, n operating at the same frequency band in the same area should be identical:

$$k_1 = \frac{\cancel{A_1 - Aw_1}}{\cancel{l_1}} \frac{Lr_1 - Aw_1}{l_1} \approx k_2 = \frac{\cancel{A_2 - Aw_2}}{\cancel{l_2}} \frac{Lr_2 - Aw_2}{l_2} \approx \cdots \approx k_n = \frac{\cancel{ALr_n} - Aw_n}{l_n}, \quad (12)$$

where ~~A~~Lr (dB) is rainfall-induced ~~attenuations~~loss, *i.e.*, the difference between total observed loss L_t and the baseline, Aw (dB) is wet antenna attenuation and l (km) is CML (sub-link) length. Assuming correct baseline identification and the same Aw for all CMLs, Aw can be directly quantified from any pair of sub-links of different lengths operating at the same frequency. The accuracy of the quantification relies on the fulfillment of the assumptions and the difference between the sub-link lengths. The larger is the length difference between the CMLs, and the smaller is the effect of an inaccurate baseline identification or dissimilar Aw within the CML pair. On the other hand, the assumption of spatially uniform rainfall is unlikely to be valid for CMLs covering a large area, *i.e.*, with contrasting lengths.

WAA is quantified at each time step by comparing the ~~attenuation~~rainfall-induced losses of the short CMLs to the ~~attenuation~~losses of the long CML. WAA after rainfall and during dew events is assumed to be equal to the total ~~attenuation. WAA evaluated for short CMLs is then related to rainfall intensity in terms of correlation. Wet antenna analysis is performed on attenuation data aggregated to 15 min.~~

~~**Rainfall estimation:** Rainfall is estimated for each sub-link using the k-R power-law model (Eq. 8) with ITU parameters and parameters derived from DSD classified as stratiform rains, alternatively. The parameters for stratiform rainfalls are used for its dominance in light and moderate autumn rainfalls in the Czech Republic. The specific attenuation k (dB km^{-1}) used as an input to the k-R model is calculated:~~

~~$$k = max\left(\frac{L_t - B - Aw_{const}}{l}, 0\right), \quad (13)$$~~

~~where L_t (dB) is the total observed loss, B (dB) is the baseline, Aw_{const} (dB) is constant WAA, and l (km) is the CML, resp. sub-link path length. The constant WAA is estimated separately for 73–74 GHz and 83–84 GHz sub-links as the median of WAA values quantified according to Eq. (12).~~

CML rainfall retrieval performance is evaluated for two sets of k-R model parameters: parameters derived from ITU recommendations and parameters obtained from DSD observations (Duebendorf) classified as stratiform. The CML quantitative precipitation estimates (QPEs) of the long CML are compared to average 15-min rainfall from rain gauges at the sites 1, 2, and 3. The QPEs of the short CMLs are compared to average 15-min rainfall from rain gauges at the sites 1, 2, and 4. The quantitative evaluation focuses on the long CML, which is sufficiently long to capture even the light rainfalls dominating the Prague data. The performance of the short CMLs is shown to demonstrate limitations related to the improper baseline and WAA identification which are, especially during light rainfalls, more pronounced by shorter CMLs. The CML QPEs are evaluated over selected rainfall events (Table 2) in terms of correlation, relative error in cumulative rainfall, and RMSE.

41 Results

4.1 Gaseous attenuation – effect of air humidity and temperature

Theoretical gaseous attenuation calculated from observed temperatures and relative humidity is highly correlated to water vapor density ($r = 0.94–0.97$) at both frequencies studied. The fluctuations in temperature affect this relation negligibly. The further evaluation, therefore, concentrates on the comparison of theoretical attenuation to attenuation observed by two sub-links of the long CML 1. To separate gaseous attenuation from other possible attenuations, only periods with no rainfall are evaluated.

Time series of theoretical and observed attenuation are compared in Fig. 5 which shows time series of attenuations smoothed by a moving average (one-week window size). The correlation between theoretical and observed attenuation is high for both sub-links ($r = 0.82–0.83$) and the long-term patterns of observed and theoretical attenuations correspond to each other quite well. Both theoretical and observed attenuations are higher during the summer period (August-September) and gradually decrease during the autumn period (October–December). The difference between mean attenuation levels in August and December is about 1 dB for the 83.5 GHz sub-link compared to only 0.7 dB for the 73.5 GHz sub-link. The theoretical and observed attenuations have similar median values for both frequencies during summer (2.11 resp. 2.12 dB for 73.5 GHz and 2.05 resp. 2.09 dB for 83.5 GHz). The theoretical and observed attenuations during autumn are about 0.3 dB higher for 73.5 GHz, compared to the 83.5 GHz sub-link (1.81 resp. 1.93 dB for 73.5 GHz compared to 1.58 resp. 1.65 dB for 83.5 GHz). The higher attenuations of the 73.5 GHz sub-link during the autumn period, in comparison to the 83.5 GHz sub-link, can be explained by dry air attenuation. Dry air attenuation of 73.5 GHz is about 0.2 – 0.3 dB higher (depending on temperature) than that of 83.5 GHz. On the other hand, higher frequency bands are more sensitive to water vapor attenuation, which is higher during summer. Different sensitivity to water vapor attenuation also causes more significant seasonal drift in the attenuation of the 83.5 GHz sub-link compared to the 73.5 GHz one.

The discrepancies between theoretical and observed attenuations are more pronounced when analyzing data at a 5-min resolution, as demonstrated on the time series of four summer days shown in Fig. 5b. This is because the separation of gaseous attenuation from the other sources of attenuation or hardware-related artifacts is challenging in real conditions. Despite these

discrepancies, the correlation between theoretical and observed attenuations remains relatively high (r = 0.70–0.72). The theoretical and observed attenuations are highly correlated during August (Fig. 6) with the correlation coefficients reaching 0.84 and 0.90 for the 73.5 GHz (1a) resp. 83.5 GHz (1b) sub-link. induced loss. The correlation is lowest during December (r = 0.36 resp. 0.16).

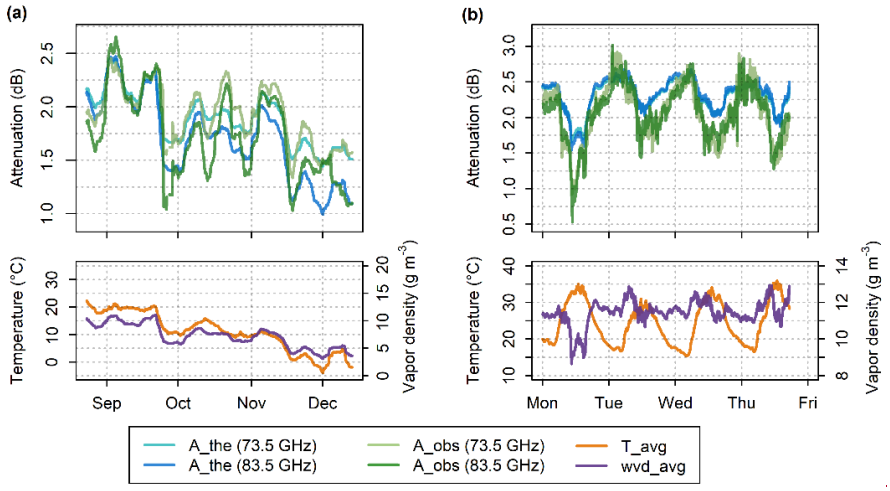

Figure 5: Theoretical and observed attenuation from the 73.5 and 83.5 GHz sub-links of CML 1 – (a) data over the whole observation period smoothed by a moving average with a window size of one week; (b) 5-min data during four summer days.

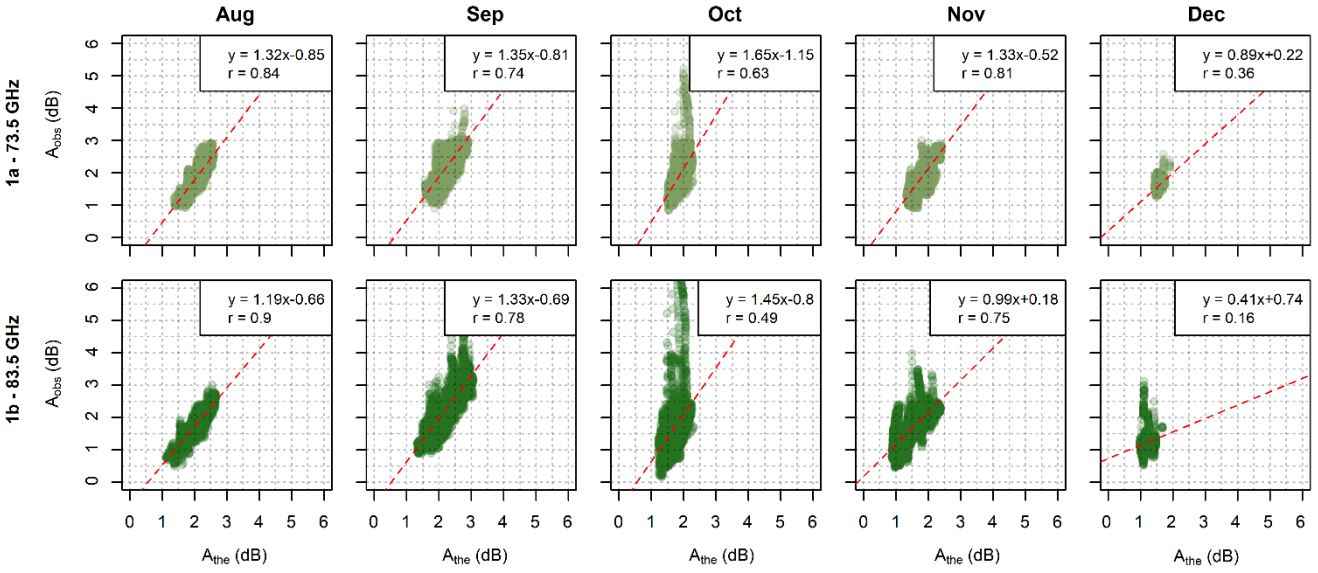

Figure. 6: Comparison of theoretical (x-axis) and observed (y-axis) gas attenuations at the 73.5 and 83.5 GHz sub-links of the CML 1 for 5-min data. Data are shown separately for each month.

4.2 Accuracy of the k-R power-law approximation

Evaluation of theoretical DSD: The relationship between attenuation and rainfall can be, for both frequencies, extremely well approximated by the power law model, however, the parameters heavily depend on DSD (Fig. 7). For example, the specific attenuation 16 dB km^{-1} corresponds to a rainfall intensity of about 30 mm h^{-1} for rainfall with DSD typical for stratiform rainfalls. However, throughout convective rainfall the same specific attenuation would occur for rainfall intensities of about 50 mm h^{-1}. For both frequencies the model using ITU parameter results between curves fitted to the rainfalls with stratiform resp. convective DSD. However, it is closer to the 'stratiform' curve for lower rainfall intensities and approximates a better 'convective' curve for intensities higher than approx. 10–15 mm h^{-1}. The ITU parameters, therefore, provide a good approximation when no information on precipitation type is available.

Evaluation on Duebendorf DSD data: Similar power-law fits are obtained when modeling attenuation and rainfall from real DSD observations. Here, two types of rainfall are classified based on mass-weighted drop diameter D_m (Eq. 10). The fitting of the classification threshold $\widehat{D_m}$ (Eq. 11) results in parameters c = 1.29 h^{-d} mm$^{1/d}$ and d = 0.16. The relation between rainfall intensity and theoretical attenuation obtained is shown, together with fitted k-R power law curves, in Fig. 8. The spread of rainfall intensity clearly grows with increasing attenuation. The k-R model deficiencies, therefore, increase with increasing rainfall intensity, as can be also seen from the RMSE values (Table 4).

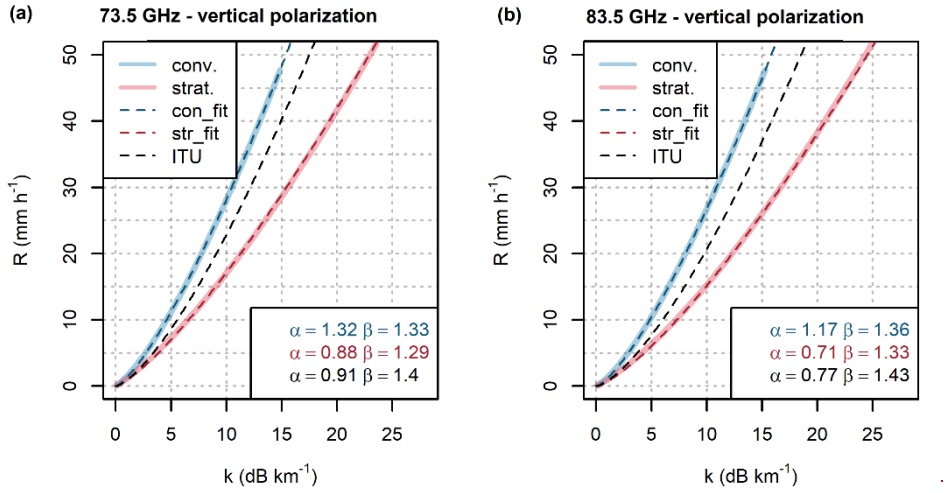

Figure 7: Attenuation-rainfall relation for vertically polarized radio waves at (a) frequency 73.5 GHz and (b) 83.5 GHz derived from theoretical DSD corresponding to stratiform and convective rainfall. A k-R model (Eq. 8) with parameters according to ITU-R (2005) lies between the curves corresponding to virtual convective and stratiform rainfalls. Parameters of the models are shown.

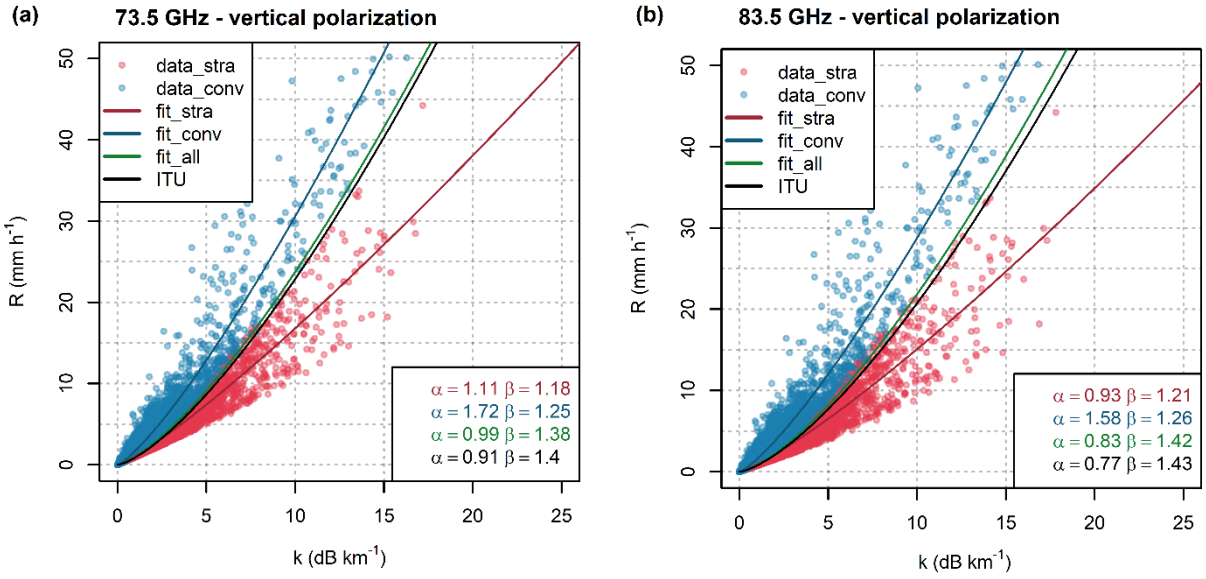

Figure 8: Relation between specific attenuation and rainfall derived from one year of DSD data for vertically polarized radio waves at (a) frequency 73.5 GHz, and (b) 83.5 GHz. The k-R model (Eq. 8) with parameters according to ITU-R (2005) resembles the model optimized for all the records. The curves optimized for convective and stratiform rainfalls differ significantly. Parameters of the models are shown.

Table 4: RMSE values measuring differences between observed and simulated rainfall using the k-R model with different parameter sets. The evaluation is provided separately for light, moderate, and heavy rainfall as well as for the whole dataset.

Parameter set	Freq. (GHz)	RMSE (mm h^{-1})			
		All data	*Light rainfall* $R \leq 4$	*Moderate rainfall* $R = 4$–12	*Heavy rainfall* $R > 12$
Separate fit	73.5	0.67	0.20	1.34	4.75
	83.5	0.73	0.24	1.48	5.08
Joined fit	73.5	1.17	0.43	2.46	8.03
	83.5	1.26	0.41	2.73	8.43
ITU	73.5	1.18	0.41	2.39	8.17
	83.5	1.27	0.45	2.63	8.74

~~4.3 Wet antenna attenuation~~

~~Figure 9~~ presents CML data at a 1-~~-~~min temporal resolution featuring: i) attenuation during peak rainfall; ii) attenuation during dry spells at night on 3rd ~~Nov.~~ November and after the rainfall; and iii) attenuations during dew occurrence on the morning of 4th ~~Nov. Attenuation~~November. Rainfall-induced loss during peak rainfall is markedly influenced by raindrop path attenuation and is proportional to path length (Fig. ~~9b~~5b). In contrast, ~~attenuation~~rainfall-induced loss both during dry spells and after a rainfall, as well as ~~attenuation~~ during dew occurrences (~~with the exception of~~except sub-link 6b) is dominated by WAA and, thus, independent of path length. Therefore, the WAA quantification method utilizing different CML path lengths ~~(section 3.5)~~ seems to be conceptually justified.

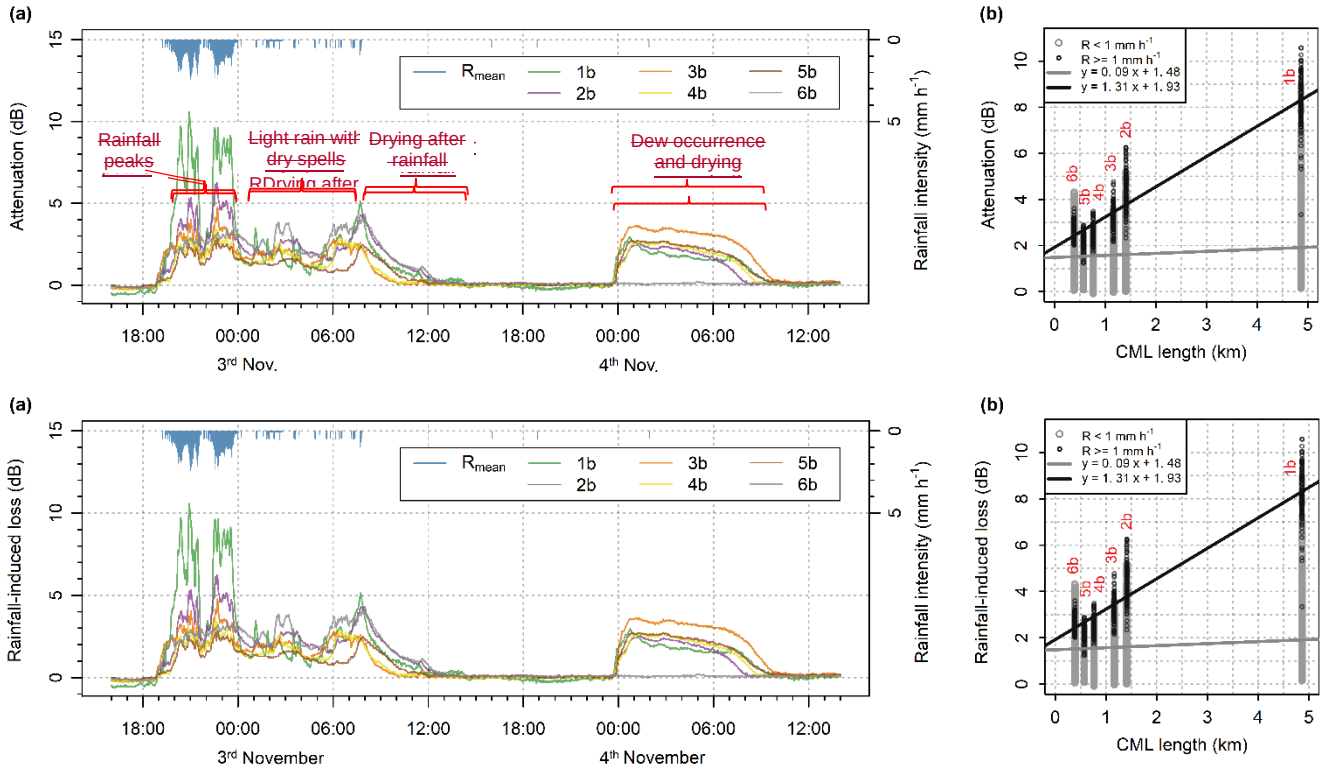

Figure ~~9~~5: (a) ~~Total rainfall~~Rainfall-induced ~~attenuation~~loss of 83–84 GHz sub-links and mean rainfall intensity from all four rain gauges. Period with peak rainfalls on 2nd ~~Nov.~~November from approx. 19:00 to 00:00, period with light rainfall and dry spells on 3rd ~~Nov.~~November from approx. 00:00 to 05:00, antenna drying period on 3rd ~~Nov.~~November from approx. 08:00 to 14:00, and dew occurrence and subsequent antenna drying on 4th ~~Nov.~~November from approx. 00:00 to 10:00. (b) ~~Total attenuation~~Rainfall-induced loss plotted against path length for 83-84 GHz sub-links with two separate linear fits for intervals with moderate rainfall and intervals with very-light rainfall including dry spells. Period from 19:00 on 2nd ~~Nov.~~November to 14:00 on 3rd ~~Nov.~~November is shown.

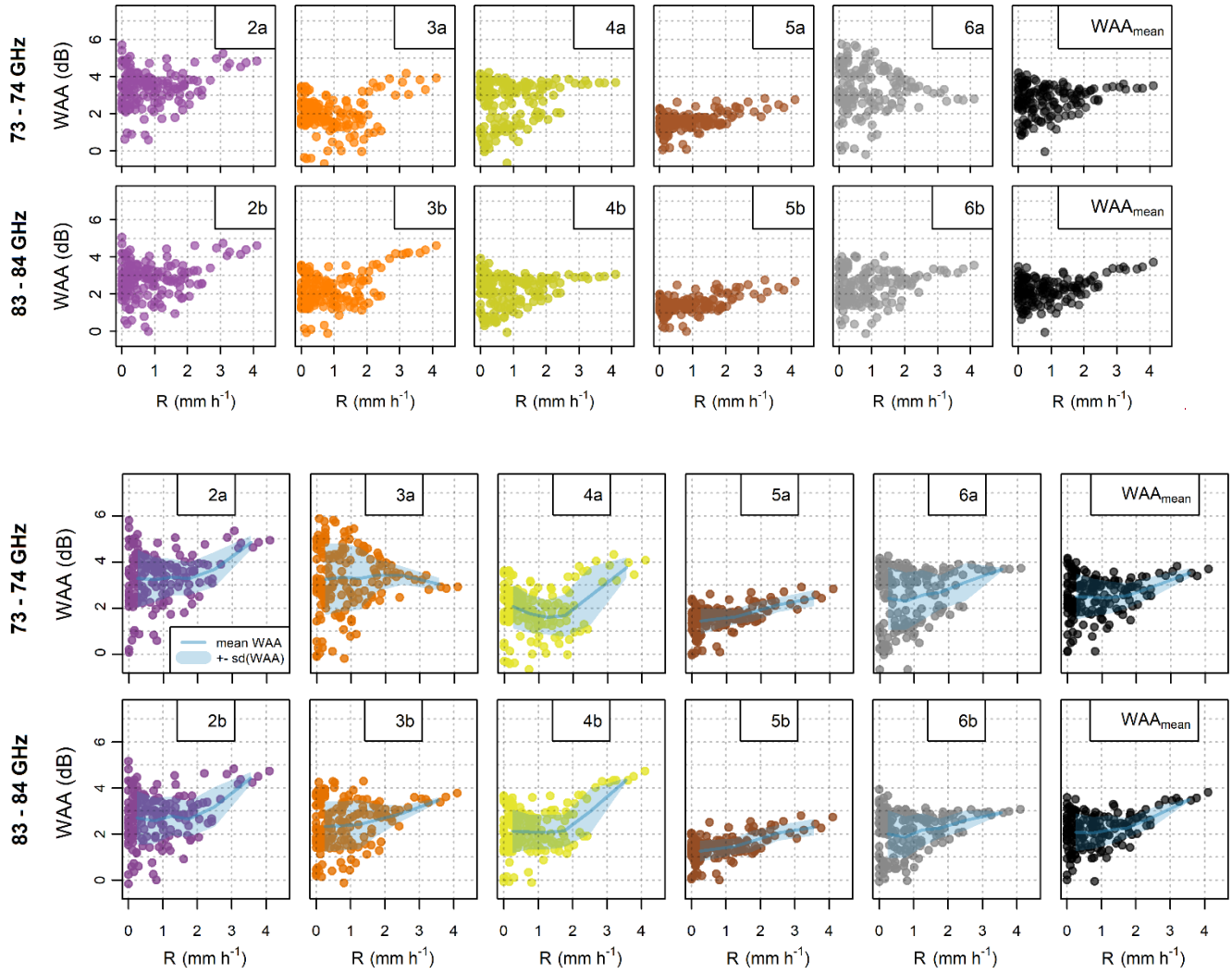

Figure ~~10~~6: Wet antenna attenuation during rainfall estimated from the differential attenuation of short and long CMLs. WAAs ~~for~~ with their mean and standard deviation are shown for both sub-links (73–74 GHz and 83–84 GHz) ~~are shown for CML~~of CMLs 1–5. The panels on the right side show mean WAA for all CMLs.

WAA quantified for each shorter CML and their average is shown in Fig. ~~10~~6 at a 15-min temporal resolution. ~~The correlation~~WAA is related to mean rainfall intensity ~~is weak except for sub-links 6a~~from rain gauges at the sites 1, 2 and ~~5b with correlation coefficients r = 0.464~~ and ~~r = 0.53, respectively.~~subdivided into bins of the size 0.5 mm h^{-1} for light rainfalls under 2 mm h^{-1}, and bins of the size 1 mm h^{-1} and 1.1 mm h^{-1} for higher rainfall intensities 2–3 mm h^{-1} resp. 3–4.1 mm h^{-1}, which are sparse in our dataset. Mean WAA and its standard deviation is quantified for each bin. Higher rainfall intensities are, in general, associated with high WAA, whereas WAA reaches a wide range of values during lower intensities. ~~WAA averaged over the whole evaluation period is between 1.60–3.47 dB~~ Mean WAA for rainfall intensities lower than 0.5 mm h^{-1} reaches for the 73–74 GHz sub-links ~~and 1.41–2.48~~1.4–3.3 dB with standard deviations 0.6–1.3 dB and for the 83–84 GHz

sub-links~~. Further, inspection of CML time series reveals that attenuation after rainfall decreases exponentially which is probably due~~ 1.3–2.7 dB with standard deviations 0.5–1.2 dB. Similar values are obtained when evaluating mean WAA and standard deviation over the whole evaluation period: Mean WAA for the 73–74 GHz sub-links is between 1.6–3.4 dB with standard deviations 0.5–1.3 dB, and 1.4–2.8 dB with standard deviations 0.5–1.1 dB for the 83–84 GHz sub-links. WAA correction used during rainfall retrieval considers WAA being a constant. It is determined as the median value of WAAs quantified separately for the 73–74 GHz resp. 83–84 GHz sub-links. This simple approach might lead to ~~the drying of the antennas (Fig. 9a, 3rd Nov).~~ systematic under- or overestimating of rainfall-induced loss in about 1 dB and random errors corresponding to standard deviations reported above.

Further, inspection of CML time series reveals exponential decrease of attenuation after rainfall, which is probably due to the drying of the antennas (Fig. 5a, 3rd November). WAA also contributes to total attenuation during the occurrence of dew when water condensates on the antenna radomes. Attenuation associated with dew deposition is similar for both frequency bands and reaches up to 4 dB (Fig. ~~9a~~5a, 4th ~~Nov~~November morning). These values are higher than WAA caused by rainfall.

~~**4.4 Rainfall estimation**~~

~~**Figure 11**~~**3.5 Water vapor detection**

The detection of water vapor from CML observations relies strongly on ability to separate gaseous attenuation from other losses. The evaluation presented in this study is limited to this aspect. The effect of temperature and air humidity on total CML attenuation is estimated theoretically from observed air temperature and relative humidity (see section 2.2) and compared to the real CML data obtained during the case study from the long CML (ID 1). Atmospheric pressure was not measured and is assumed to be constant corresponding to 1013 hPa. Atmospheric pressure changes related to weather conditions have, however, an almost negligible effect on theoretical attenuation (ITU-R, 2019). The temperature and air humidity used in the analyses are averages from the observations at two locations along the CML path. Gaseous attenuation is estimated for the period from 20th August to 16th December 2018 and only considers dry weather, as defined in section 3.2.

The theoretical attenuation derived from air temperature and relative humidity observations is compared to the observed attenuation of the long CML. To enable a comparison, the observed attenuation is also aggregated to a 5-min time step corresponding to the time step of temperature and humidity observations, resp. theoretical attenuation.

The observed attenuation patterns are compared to the theoretical patterns calculated from temperature and air humidity observations. The agreement between theoretical and observed attenuation is quantified in terms of correlations, mean difference, root mean square error (RMSE), and their amplitudes. In addition, seasonal drift is demonstrated on time series smoothed by a moving average with a window size of one week.

3.6 CML rainfall retrieval

Rainfall is estimated for each sub-link using the k-R power-law model (Eq. 9) with ITU parameters and parameters derived from DSD observations (Duebendorf data) classified as stratiform rains, alternatively. The parameters for stratiform rainfalls are used for its dominance in light and moderate autumn rainfalls in the Czech Republic. The CML quantitative precipitation estimates (QPEs) of the long CML are compared to average 15-min rainfall from rain gauges at the sites 1, 2, and 3. The QPEs of the short CMLs are compared to average 15-min rainfall from rain gauges at the sites 1, 2, and 4. The quantitative evaluation focuses on the long CML, which is sufficiently long to capture even the light rainfalls dominating the Prague data. The performance of the short CMLs is shown to demonstrate limitations related to the inappropriate baseline and WAA identification which are, especially during light rainfalls, more pronounced by shorter CMLs. The CML QPEs are evaluated over selected rainfall events (Table 2) in terms of correlation, relative error in cumulative rainfall, and RMSE.

Uncertainty estimation: CML QPEs are subdivided into bins having size 0.5 mm h^{-1} for light rainfalls under 2 mm h^{-1}, two other larger bins (2–3 mm h^{-1} and 3–4.1 mm h^{-1}) are defined for higher rainfall intensities, which are sparse in our dataset. Average difference between CML QPEs and mean rain-gauge rainfall and standard deviations of residuals are then quantified for each bin. Evaluation of DSD-related deficits of k-R model is, for simplicity, limited to k-R model with ITU parameters and assumes that drop size spectra of rainfalls during evaluation period resembles Duebendorf DSD classified as stratiform. Expected systematic and random deviations of the k-R model with ITU parameters are quantified in section 3.3 for bins of specific attenuation. Nevertheless, these bins need to be transformed to rainfall intensity to enable comparison with quantified deviations of CML QPEs. Eq. (9) with parameters for stratiform rainfalls is used for this purpose. The estimation of WAA related deficiencies is limited to systematic errors and assumes that the WAA offset (2.3 and 2.7 dB) might be for any CML systematically under- or overestimated by ± 1 dB. First, CML QPEs are calculated for specific attenuations in the range of 0–4 dB km^{-1} using the k-R model (Eq. 9) with parameters for stratiform rainfalls. Second, the systematic deviation ± 1 dB is introduced into Eq. (3) and systematically under- and overestimated QPEs are calculated (Eq. 9) for each CML considering differences in their path lengths. Difference between unbiased QPEs (corresponding to mean rain-gauge rainfall) and under- and overestimated QPEs is quantified and related to rainfall intensity.

4 Results

4.1 Gaseous attenuation – effect of air humidity and temperature

Theoretical gaseous attenuation calculated from observed temperatures and relative humidity is positively correlated to water vapor density (r = 0.94–0.97) at both frequencies studied. The fluctuations in temperature affect this relation negligibly. The further evaluation, therefore, concentrates on the comparison of theoretical attenuation to attenuation observed by two sub-links of the long CML 1. To separate gaseous attenuation from other possible attenuations, only dry-weather periods are evaluated.

Time series of theoretical and observed attenuation are compared in Fig. 7, which shows time series of specific attenuations smoothed by a moving average (one-week window size). The correlation between theoretical and observed attenuation is high for both sub-links (r = 0.82–0.83) and the long-term patterns of observed and theoretical attenuations correspond to each other quite well. Both theoretical and observed attenuations are higher during the summer period (August-September) and gradually decrease during the autumn period (October–December). The difference between mean attenuation levels in August and December is about 0.15 dB km^{-1} for the 83.5 GHz sub-link compared to only 0.12 dB km^{-1} for the 73.5 GHz sub-link. The theoretical and observed attenuations have similar median values for both frequencies during summer (0.44 resp. 0.43 dB km^{-1} for 73.5 GHz and 0.43 resp. 0.42 dB km^{-1} for 83.5 GHz). The theoretical and observed attenuations during autumn are about 0.06 dB km^{-1} higher for 73.5 GHz, compared to the 83.5 GHz sub-link (0.37 resp. 0.40 dB km^{-1} for 73.5 GHz compared to 0.32 resp. 0.33 dB km^{-1} for 83.5 GHz).

The higher attenuations of the 73.5 GHz sub-link during the autumn period, in comparison to the 83.5 GHz sub-link, can be explained by dry-air attenuation. Dry-air attenuation of 73.5 GHz is about 0.04–0.06 dB km^{-1} higher (depending on temperature) than that of 83.5 GHz. On the other hand, higher frequency bands are more sensitive to water-vapor attenuation, which is higher during the summer. Different sensitivity to water-vapor attenuation also causes more significant seasonal drift in the attenuation of the 83.5 GHz sub-link compared to the 73.5 GHz one.

The discrepancies between theoretical and observed attenuations are more pronounced when analyzing data at a 5-min resolution, as demonstrated on the time series of four summer days shown in Fig. 7b. This is because the separation of gaseous attenuation from the other sources of attenuation or hardware related artifacts is challenging in real conditions. Despite these discrepancies, the correlation between theoretical and observed attenuations remains relatively high (r = 0.70–0.72). The theoretical and observed attenuations are highly correlated during August (Fig. 8), with the correlation coefficients reaching 0.84 and 0.90 for the 73.5 GHz resp. 83.5 GHz sub-link. The correlation is lowest during December (r = 0.36 resp. 0.16). On the other hand, systematic deviations are largest during August, where observed attenuation of 73.5 an 83.5 GHz sub-links is underestimated by 0.03 resp. 0.05 dB km^{-1} compared to theoretical attenuation. RMSE is for both sub-links largest during October (0.08–0.13 dB km^{-1}). Possible causes of outlying observed attenuations causing high RMSEs are discussed in section 5. The lowest RMSE is quantified for 73.5 GHz sub-link during December and for 83.5 GHz sub-link during August.

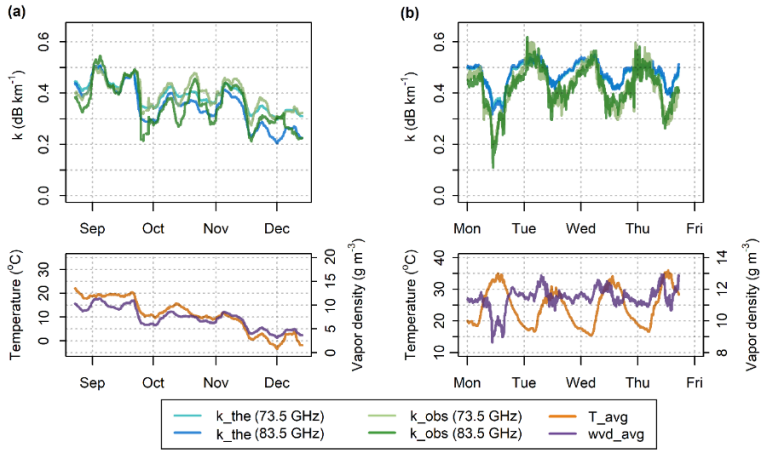

Figure 7: Theoretical and observed specific attenuation from the 73.5 and 83.5 GHz sub-links of CML 1 and observed temperature and water vapor density – (a) data over the whole observation period smoothed by a moving average with one-week window; (b) 5-min data during four summer days.

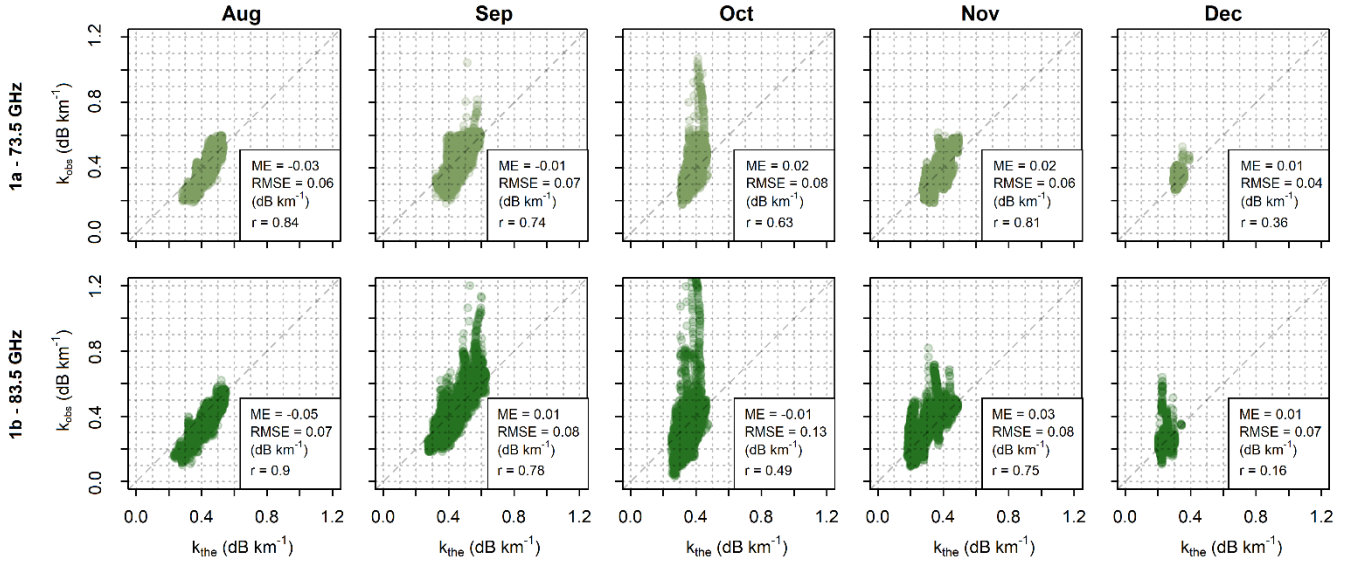

Figure 8: Comparison of theoretical (x-axis) and observed (y-axis) gas specific attenuations at the 73.5 and 83.5 GHz sub-links of the CML 1 for 5-min data. Data are shown separately for each month.

4.2 Rainfall estimation

Figure 9 shows QPEs obtained from CMLs using the k-R model with ITU parameters and parameters derived from DSD during rainfalls classified as stratiform. Note that DSD is obtained from the independent Duebendorf dataset. The long CML, in particular the 83.5 GHz sub-link, is capable of capturing even light rainfall intensities reliably. The correlation to rain-gauge observations is excellent ($r \approx 0.96$). However, QPEs derived with ITU parameters tend to underestimate light rainfalls, ~~which also leads~~leading to increased RMSE (Table ~~5~~3). The model with DSD-derived parameters improves performance with respect to all metrics. Sub-link 1a also remains significantly underestimated with DSD-derived parameters. ~~This is due to deficits in~~

~~the baseline and WAA identification.~~ The underestimation is pronounced especially during very light rainfalls with rainfall intensities under 1 mm h^{-1}, which represent 25 % of total rainfall depth. ~~Shorter CMLs are less sensitive to rainfall along their shorter path and are more affected by deficiencies in the estimated baseline and WAA. Thus,~~The use of DSD parameters does not significantly improve performance of short CMLs~~.~~ and CMLs shorter than 1 km overestimate rainfall intensities more than longer CMLs.

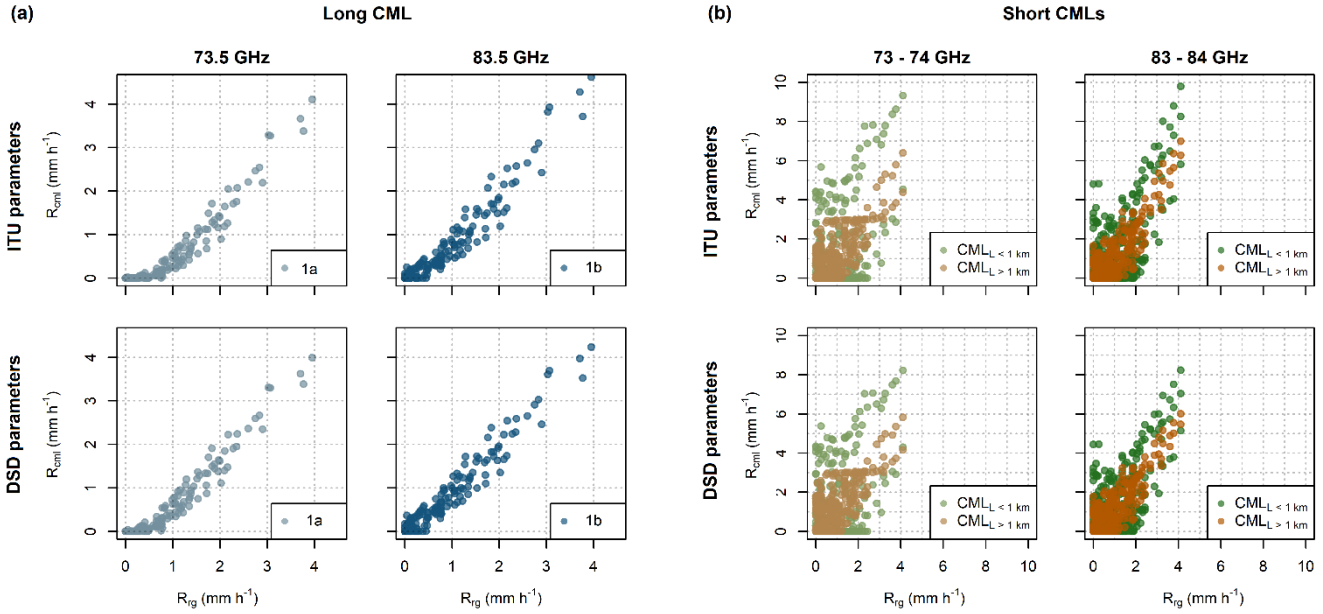

Figure ~~11~~9: CML QPEs for the long CML (a) and short (b) CMLs when using k-R model with ITU (top) and DSD-derived (bottom) parameters. Results are shown for both frequency ranges. QPEs for short CMLs are differentiated by color into two groups to depict CMLs with path lengths shorter and longer than 1 km separately.

Systematic and random deviations of CML QPEs are evaluated quantitatively in Figure 10 and compared to expected systematic and random deviations i) due to deficits of the constant WAA model and, ii) due to DSD-related deficits of the ITU-based model. The expected errors due to DSD are independent of CML path length and contribute equally to all the CMLs. In contrast, expected errors due to WAA are much more pronounced by the shorter CMLs and can explain most of their errors. Regarding the 4.86-km-long CML, DSD seems to affect deviations of QPEs similarly or even more (for the 83.5 GHz sub-link) than WAA. DSD-related errors might explain by this CML substantial part of observed systematic deviations. Interestingly, expected random error due to DSD variability is even larger than observed variability in QPEs during rainfalls intensities higher than approx. 2–3 mm h^{-1}. Note, that observed variability for rainfall intensities higher than 3 mm h^{-1} is by the longest CML quantified based on five observations only.

In general, sensitivity to rainfall, which is proportional to a CML path length, seems to be crucial characteristic influencing the accuracy of CMLs when observing light rainfalls under 2 mm h^{-1}. For heavier rainfalls, other characteristics than path length specific to each CML influence the uncertainties more significantly. For example, CML 5, which is less biased than

longer CML 4, is relatively insensitive to WAA (Fig. 6) compared to the other CMLs. In addition, the WAA quantified for CML 5 is more correlated with rainfall intensity (r = 0.47 and 0.54 for the sub-link 5a resp. 5b) than by the other CMLs (r = 0.23–0.40 for all the sub-links).

Table ~~5~~3: Performance metrics of the CML QPEs obtained with the k-R model using ITU and DSD-derived parameters

Sub-link	ITU parameters			DSD parameters		
id	r (-)	rel. error (-)	RMSE (mm h^{-1})	r (-)	rel. error (-)	RMSE (mm h^{-1})
1a	0.95	-0.44	0.49	0.96	-0.35	0.39
1b	0.96	-0.17	0.31	0.97	-0.08	0.24
2a	0.86	0.10	0.64	0.86	0.23	0.64
2b	0.87	0.26	0.75	0.87	0.33	0.69
3a	0.67	0.34	0.92	0.66	0.43	0.97
3b	0.84	0.15	0.71	0.83	0.21	0.69
4a	0.74	-0.48	0.95	0.74	-0.44	0.92
4b	0.78	0.24	1.31	0.77	0.26	1.14
5a	0.73	-0.78	0.92	0.74	-0.77	0.90
5b	0.80	-0.61	0.79	0.81	-0.59	0.76
6a	0.57	1.26	2.29	0.53	1.25	2.18
6b	0.63	0.61	1.56	0.61	0.59	1.44

~~In general, rainfall retrieval by E-band CMLs is affected during light rainfalls not only by deficiencies related to WAA and the baseline, but also deficiencies related to DSD. WAA and baseline-related errors clearly dominate by shorter CMLs, whereas regarding the 4.86-km-long CML, DSD seems to have a similar or even larger effect (in the case of the 83.5 GHz sub-link). The effect of DSD is likely to increase with high rainfall intensities, which were, however, not encountered during the case study period.~~

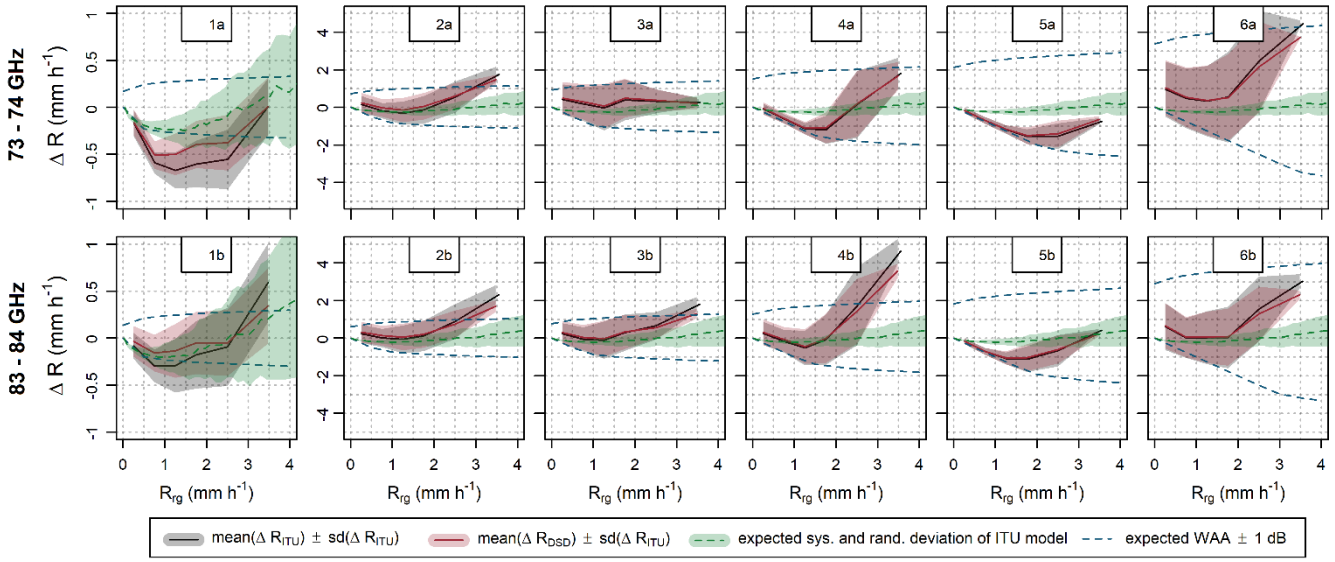

Figure 10: Deviations of CML QPEs when using k-R model with ITU parameters and DSD-derived parameters for stratiform rainfalls. Expected deviations due to DSD and deficits in constant WAA model are also shown. Note the different scale of y-axis for the long (1 a, b) and the short (2-6 a, b) sub-links.

5 Discussion

~~**Gaseous attenuation:** The theoretical gaseous attenuation for 73.5 GHz sub-link ranges between 1.33 dB and 2.90 dB (amplitude 0.33 dB km^{-1}) and for the 83.5 GHz sub-link between 0.95 dB and 3.06 dB (amplitude 0.45 dB km^{-1}). These fluctuations have a minor effect on rainfall retrieval (with respect to uncaptured baseline variability), as 0.33, resp. 0.45 dB km^{-1} corresponds to a rainfall intensity of about 0.19 mm h^{-1} resp. 0.25 mm h^{-1} for 73.5 GHz and 83.5 GHz sub-links. On the other hand, this signal is sufficiently strong to enable the detection of water vapor at long CMLs, as 0.33 dB km^{-1} and 0.45 dB km^{-1} corresponds by the long CML (4.86 km) of 1.60 dB resp. 2.19 dB. The major challenge lies in the separation of gaseous attenuation from losses caused by other phenomena. This is easier during periods without rainfall, nevertheless, the following causes of losses need to be identified and separated.~~

~~First, WAA occurring after rainfall and during dew events can reach 4 dB, *i.e.*, substantially exceeds the gaseous attenuation. Here, a safety window of 6 h size was used before and after each rain gauge tipping to exclude periods with WAA contribution. This mostly eliminated WAA before and after rainfall events and WAA during strong dew events causing a rain gauge tip. However, such eliminations considerably reduce ratio of time intervals with observations. Moreover, periods before and after rainfalls might have higher relative humidity than average and discarding those from the evaluation leads to potentially biased long-term estimates of water vapor density.~~

~~Second, signal fluctuations due to multipath propagation or other sources of uncertainty might affect the observed attenuation level. Multipath interferences often lead to a decreased signal power level of one sub-link while keeping the signal power level of the other sub-link (Valtr et al., 2011).~~

~~Finally, hardware related artifacts might destroy a gaseous attenuation signal. For example, sub-link 6a drifts about 1.5 dB during the period from the end of October to mid-December. This drift is clearly related to the hardware as the total loss due to gaseous attenuation along the path length of 0.39 km can reach only about 0.13 dB. Such a drift would, however, make the quantification of gaseous attenuation impossible even at long CMLs.~~

~~The separation of gaseous attenuation from other sources of signal loss is challenging. Further research could take advantage of the 10 GHz duplex separation between the sub-links of E-band CMLs. Combining attenuation information from CMLs of different lengths might also be promising.~~

~~**Accuracy of the k-R power law approximation:** The relation between rainfall and raindrop attenuation (Eq. 7 and 8) on E-band frequencies is substantially more dependent on DSD than on 15–40 GHz CMLs (Chwala, 2017). The parameters of the power law model (Eq. 8), when optimized for all the DSD data, corresponds extremely well to the ITU parameters (ITU-R, 2005). However, high values of RMSE results from the variability in DSD when using one fit for all the records. Separate fits for convective and stratiform rainfalls halve the RMSE values. Moreover, the separate power law fits are closer to linear (parameter β between 1.18 and 1.26, compared to β between 1.38 and 1.4) and are less prone to errors related to non-uniform rainfall distribution along the CML path. Errors due to non-linearity of Eq. (8) might be reduced by reconstructing rainfall spatial variability along the CML path from the neighboring CMLs, or by introducing a climate-based relation between the non-uniformity of rainfall distribution and rainfall intensity. Such methods will, however, require further research. In general, unknown DSD will probably be one of the major uncertainties in quantitative estimates of heavy rainfall. On the other hand, high sensitivity to DSD creates the opportunity to infer information on DSD from the attenuation of E-band CMLs, *e.g.*, in a condensed form of DSD moments. This is, in theory, also possible at 15–40 GHz, though difficult to accomplish in practice (Leth et al., 2019). Additional information on rainfall intensity or a combination with attenuation data of CMLs operating at lower frequencies will be required for DSD retrieval.~~

Quality check before rainfall retrieval: Quality check was performed through visually inspecting time series of total losses. In the case of CML 2 a sudden change in the baseline by 2 dB was manually corrected. More details to hardware related artifacts ~~is~~are provided in *Appendix B*.

Dry-wet weather classification and baseline separation:

The dry-wet classification has been reported as an important step in CML pre-processing as it minimizes unwanted changes in attenuation level by setting the baseline separately for each event from the relatively short period before the event (Chwala and Kunstmann, 2019; Overeem et al., 2011). Here, dry-wet weather classification was not used for baseline identification~~.~~ when retrieving rainfall. It was a pragmatic choice enabling better descriptions of the WAA effect. Dry-wet classification is also needed for filtering out periods with increased attenuation due to WAA (after rainfall and during dew events), nevertheless, these periods are in the event-based evaluation not included.

The separation of wet weather (including dew occurrence) was identified as a crucial step when analyzing attenuation due to water vapor. When rain gauges are not available, a CML-based classification needs to be performed. The dry-wet weather classification (Schleiss and Berne, 2010) used in *Appendix A* is designed to identify rainy periods and consider dew occurrences as dry weather. Although sensitivity to dew events can be increased by optimizing the parameters of the algorithm, dew events have similar dynamics as changes in air humidity as they are both dependent on temperature. Thus, other methods also considering observations of neighboring CMLs (Overeem et al., 2011) might be more appropriate for the dry-wet weather classification used ~~for the separation of~~to separate attenuation caused by water vapor.

The baseline identification method with a moving median (without dry-wet weather classification) performed well for rainfall retrieval purposes. It should be noted that, ~~with the exception of~~except for one case, the observed attenuation levels were stable. The ~~median moving window~~ baseline identified by moving median with ~~window size of~~ one- week window was capable ~~to correct~~correcting long-term drift, which occurred on sub-link 6a (*Appendix B*). ~~Window size of one~~ One-week window is sufficiently long to not include more than 50 % of wet weather records into the window at any time step in the temperate climate. However, the median moving window baseline is not suitable for distinguishing between long-term drift related to hardware malfunction (*e.g.*, sub-link 6a) and drift related to seasonal changes in air humidity and temperature (sub-links 1a and 1b). Constant baseline was, therefore, used for analysis of gaseous attenuation on sub-links 1a and 1b instead. Possible water vapor monitoring thus poses higher requirements on the hardware with respect to the stability of the attenuation baseline.

~~Wet~~**Accuracy of the k-R power law approximation:** The relation between rainfall and raindrop attenuation (Eq. 8 and 9) on E-band frequencies is substantially more dependent on DSD than on 15–40 GHz CMLs (Chwala, 2017). The parameters of the power-law model (Eq. 9), when optimized for all the DSD data, corresponds exceptionally well to the ITU parameters (ITU-R, 2005). However, random errors resulting from the variability in DSD are high when using one fit for all the records. Separate fits for convective and stratiform rainfalls reduce these errors. Moreover, the separate power-law fits are closer to linear (parameter β between 1.18 and 1.26, compared to β between 1.38 and 1.4) and are less prone to errors related to non-uniform rainfall distribution along the CML path. On the other hand, high systematic errors will occur for misclassifying rainfall type (DSD). Errors due to non-linearity of Eq. (9) might be reduced by reconstructing rainfall spatial variability along the CML path from the neighboring CMLs, or by introducing a climate-based relation between the non-uniformity of rainfall distribution and rainfall intensity. Such methods will, however, require further research. In general, unknown DSD will probably be one of the significant uncertainties in quantitative estimates of heavy rainfall. On the other hand, high sensitivity to DSD creates the opportunity to infer information on DSD from the attenuation of E-band CMLs, *e.g.*, in a condensed form of DSD moments. This is, in theory, also possible at 15–40 GHz, though challenging to accomplish in practice (Leth et al., 2019). Additional information on rainfall intensity or a combination with attenuation data of CMLs operating at lower frequencies will be required for DSD retrieval.

Quantification of wet antenna attenuation: Quantification of WAA during rainfall is based on the assumption that rainfall has a uniform distribution over the study area, and that water formation on the surface of antenna radomes is the same for both the short CMLs and the long one. In our case, the first assumption holds well as all four rain gauges observe similar rainfall

intensities during the evaluated events. The correlation coefficient between rain gauges at sites 1, 2, and 4, which are closer to each other, is 0.94–0.96 and 0.88–0.93 for the more distant rain gauge at site 3. The standard deviation between mean rainfall intensity and rainfall intensities observed by single rain gauges reaches 0.15–0.36 mm h^{-1}, being lowest for lightest rainfalls and slightly grows with increasing rainfall intensity. The similarity in antenna characteristics, *i.e.* hydrophobic properties of antenna radomes ~~as well as~~and their actual status, was not inspected directly. That said, the estimation procedure is relatively insensitive to WAA occurring on the long CML as attenuation along its path dominates over WAA, even during relatively light rainfalls and, thus, WAA does not significantly influence the estimated specific attenuation (~~13~~Eq. 3).

WAA during rainfall is weakly correlated to rainfall intensity (*e.g.*, Schleiss et al., 2013). Our results are limited to light and moderate rainfall only. Schleiss et al. (2013) reported drying of up to six hours with an exponential decrease of WAA, which also corresponds well to our observations (Fig. ~~9a~~5a). However, quantification of exact ~~durations~~duration of drying ~~require~~requires additional instrumentation to enable us to determine the ends of rainfalls directly. The exponential WAA decrease during drying was also reported by Leth et al. (2018), who suggested that this drying pattern occurs on antennas with non-degraded coating, which is also the case of the CML antennas analyzed. On the other hand, WAA attenuation patterns on antennas with degraded coating might be markedly different.

WAA, due to water vapor condensation, reaches higher values than during light rainfall. This might be caused by an absence of water rivulets (Leth et al., 2018). The higher values of attenuation caused by water droplets, in comparison to attenuation caused by rivulets, was also reported by Mancini et al. (2019). Comparable attenuation patterns of light rainfall and water vapor condensation may cause the misclassification of dew as rainfall.

In general, WAA quantified in this study is slightly higher than WAA reported for lower frequencies (Leth et al., 2018). However, the relative contribution of WAA to the total attenuation is less significant (given the high sensitivity of CMLs to raindrop path attenuation). WAA is, thus, a smaller source of possible bias than on 15–40 GHz frequencies~~, nevertheless, its~~. Nevertheless, accurate quantification of WAA is still ~~important~~essential, especially for shorter CMLs. In addition, WAA during heavy rainfalls was not investigated in this study and might be higher, as was shown for lower frequencies by Fencl et al. (2019).

Gaseous attenuation: The theoretical gaseous attenuation for 73.5 GHz sub-link ranges between 0.27 dB km^{-1} and 0.60 dB km^{-1} (amplitude 0.33 dB km^{-1}) and for the 83.5 GHz sub-link between 0.20 dB km^{-1} and 0.63 dB km^{-1} (amplitude 0.43 dB km^{-1}). These fluctuations have a minor effect on rainfall retrieval (with respect to uncaptured baseline variability), as 0.33, resp. 0.43 dB km^{-1} corresponds to a rainfall intensity of about 0.19 mm h^{-1} resp. 0.25 mm h^{-1} for 73.5 GHz and 83.5 GHz sub-links. On the other hand, this signal is sufficiently strong to enable the detection of water vapor at long CMLs, as 0.33 dB km^{-1} and 0.43 dB km^{-1} corresponds by the long CML (4.86 km) of 1.60 dB resp. 2.09 dB. The major challenge lies in the separation of gaseous attenuation from losses caused by other phenomena. This is easier during periods without rainfall, nevertheless, the following causes of losses need to be identified and separated.

First, WAA occurring after rainfall and during dew events can reach 4 dB, *i.e.*, substantially exceeds the gaseous attenuation. Here, a safety window of 6 h was used before and after each rain gauge tipping to exclude periods with WAA contribution.

This mostly eliminated WAA before and after rainfall events and WAA during strong dew events causing a rain-gauge tip. However, such eliminations considerably reduce the ratio of time intervals with observations. Moreover, periods before and after rainfalls might have higher relative humidity than average and discarding those from the evaluation leads to potentially biased long-term estimates of water vapor density.

Second, signal fluctuations due to multipath propagation or other sources of uncertainty might affect the observed attenuation level. Multipath interferences often lead to a decreased signal power level of one sub-link while keeping the signal power level of the other sub-link (Valtr et al., 2011).

Finally, hardware related artifacts might destroy a gaseous attenuation signal. For example, sub-link 6a drifts about 1.5 dB from the end of October to mid-December. This drift is clearly related to the hardware as the total loss due to gaseous attenuation along the path length of 0.39 km can reach only about 0.13 dB. Such a drift would, however, make the quantification of gaseous attenuation impossible even at long CMLs.

The separation of gaseous attenuation from other sources of signal loss is challenging. Further research could take advantage of the 10 GHz duplex separation between the sub-links of E-band CMLs. Combining attenuation information from CMLs of different lengths might also be promising.

Rainfall estimation: The E-band CMLs proved to be markedly more sensitive to raindrop path attenuation than 15–40 GHz devices. The long CML provided surprisingly accurate rainfall estimates, even for light rainfalls lower than 1 mm h^{-1} in intensity (Fig. ~~11~~9). Assuming a detection threshold of 1 dB (typical *tx* power quantization of older devices), a 1-km-long 83 GHz CML can already detect rainfall intensity of 0.6–1 mm h^{-1} depending on rainfall type, whereas, *e.g.*, a 23 GHz or 38 GHz CML only detects rainfalls heavier than 8.4 resp. 3.6 mm h^{-1}, *i.e.*, the sensitivity to light rainfalls is almost an order of magnitude higher for E-band CMLs. Moreover, the quantization of *rx* and *tx* records has improved to 0.1 dB with E-band CMLs. On the other hand, long E-band CMLs are prone to outages (*rx* drops under detection level) during heavy rainfall. This high sensitivity to rainfall, together with improved quantization, opens the opportunity for monitoring rainfall with CMLs having a sub-kilometer path length, which was practically not possible before without adjusting CML QPEs to the rain gauges (Fencl et al., 2017). Short CMLs are more affected by errors related to WAA, yet the influence of WAA is relatively smaller during heavier rainfall, which, however, did not occur during the evaluation period. The use of short CMLs may be convenient, especially during heavy rainfalls associated with high spatial variability by which an assumption about uniform rainfall distribution along a CML path is more likely valid than for long CMLs. Reliable rainfall estimation from short CMLs, however, requires further research on WAA modeling at E-band frequencies.

Limitations of this study: The study investigates the weather monitoring capabilities of E-band CMLs on a dataset comprised of four months of attenuation data from six Ericsson MINILINK CMLs operated within cellular backhaul. The number of CMLs and length of the period is sufficient to demonstrate the challenges and opportunities related to rainfall and water vapor monitoring at an E-band. However, the limited size of the dataset does not enable us to draw strong conclusions on the overall reliability of weather monitoring with an E-band, nor to investigate in detail new opportunities related to CML sensitivity to water vapor and DSD.

Specifically, the dataset does not include heavy rainfalls. The reliability of E-band CML rainfall estimation for heavy rainfalls is based only on ~~the evaluation of~~evaluating theoretical attenuations obtained from DSD observations (Duebendorf). The DSD effect on the attenuation-rainfall relation could not be, therefore, studied in detail on the observed CML data. Finally, air temperature and humidity are measured at two locations close to one node of the CML path. Despite these limitations, we believe that the presented results reliably demonstrate new challenges and opportunities of E-band CML weather monitoring.

6 Conclusions

E-band microwave links are increasingly updating and frequently replacing the older hardware of backhaul networks operating mostly at 15–40 GHz. This investigation demonstrates new challenges and opportunities related to CML weather monitoring. The principles behind weather retrieval ~~is~~are the same as for lower frequency bands, nevertheless the influence of atmospheric phenomena such as drop size distribution~~,~~ or changes in air temperature and humidity affect radiowave propagation in a significantly different manner. Furthermore, the hardware used by E-bands is different (quantization, accuracy, antenna wetting, etc.). The results, obtained from simulations and the case study with attenuation data from real-world CMLs, are encouraging. The main conclusions are listed below:

- E-band CMLs are markedly more attenuated by raindrops along their path than older 15–40 GHz devices, during lighter rainfalls by about 20 times more than 15 GHz and 2 - 3 times more than 40 GHz devices. This significantly improves the ability of E-band CMLs to quantify rainfall intensity accurately during light rainfalls.
- The rainfall retrieval at E-band frequencies is less influenced by wet antenna attenuation than at lower frequencies. WAA observed in this study has a similar pattern as that described by Schleiss et al. (2013), *i.e.*, it is almost uncorrelated with rainfall intensity and exhibits an exponential decrease after rainfall lasting up to several hours. WAA during dew occurrences reaches up to 4 dB.
- The power-law approximation of the attenuation-rainfall relation depends substantially more on DSD than on 15–40 GHz frequencies. The variability in DSD represents significant uncertainties in E-band CML rainfall retrieval. ~~Use~~The use of different parameter sets for different types of rainfall, as done with weather radars, reduce DSD-related errors, nevertheless this requires additional information on rainfall type.
- The k-R relation at E-band frequencies is less linear than at lower frequencies. This might cause errors in CML QPEs, especially by longer CMLs, for which a uniform distribution of rainfall intensity along their path cannot always be assumed. On the other hand, even short (sub-kilometer) E-band CMLs are sufficiently sensitive to raindrop path attenuation ~~to be used~~ for rainfall retrieval.
- Gaseous attenuation at E-band CMLs is detectable, however, it is substantially smaller than attenuation due to rainfall. Fluctuations in specific attenuation caused by water vapor typically not exceed 1 dB km^{-1} in the region of temperate climate. This magnitude is reached by rainfall with intensity around 1 mm h^{-1}. Gaseous attenuation is driven mainly by water vapor density and is, thus, in theory, an accurate predictor of this atmospheric variable. This, however, requires the efficient separation of attenuation from other signal losses which is, in practice, challenging. Our first

results show that this separation is, to some extent, possible during dry weather periods, if a sufficiently long CML (several km) is available.

In general, the ongoing shift of CML networks towards higher frequencies creates opportunities ~~for the monitoring of~~to monitor rainfall on a qualitatively different level. New E-band CMLs ~~are able to~~can observe light rainfalls and, in combination with lower frequency CMLs, potentially serve as DSD predictors. The rainfall retrieval methods developed for CMLs operating at 15–40 GHz frequencies proved to be useful for E-band CMLs ~~as well~~. Water vapor retrieval from E-band CMLs having a path length of several kilometers might be possible~~, although~~. However, the efficient separation of gaseous attenuation from other signal losses will be challenging in practice. This first experience with E-band CML weather retrieval, as presented in this study, will hopefully contribute to more robust designs of future experimental studies and case studies investigating this new technology ~~with respect~~concerning to weather monitoring.

Appendix A – Dry-wet weather classification

The classification is performed separately for each sub-link on quality-checked total observed losses. The algorithm of Schleiss and Berne (2010) is used which is based on a moving window standard deviation. The window size is set to 15 minutes and the threshold for classifying the record as wet (σ_0) is set to the 94 % quantile of all standard deviations resulting from the moving window filter. The 94 % probability corresponds approximately to the wet weather ratio in the Prague data ~~as~~ classified by the rain gauges.

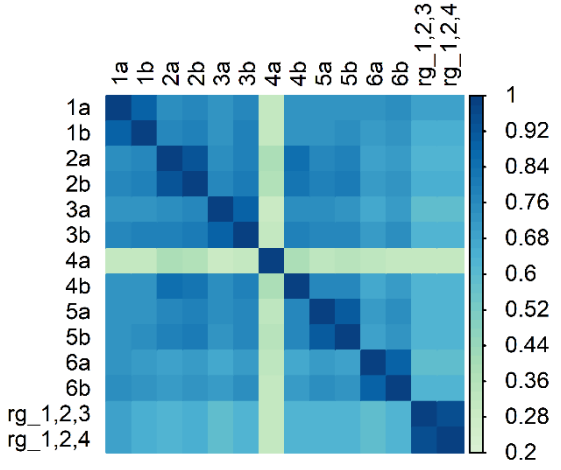

Figure A1: Statistical relationship between dry-wet classifiers based on single CML sub-links and rain gauges along the path of the long CML (rg_1,2,3) and three rain gauges near five shorter CMLs (rg_1,2,4) expressed by correlation coefficient.

Dry-wet weather classifiers obtained from CML sub-links are compared with each other and with classifiers obtained from rain gauge observations. Correlation is used here as a measure of similarity. The evaluation of dry-wet weather is performed on one-minute data because precise identification of the onset and ending of rainfall significantly affects baseline identification methods based on dry wet classification, as well as the quantification of wet antenna attenuation.

Dry-wet weather classifiers of single sub-links belonging to one CML are strongly correlated (Fig. A1). An exception is sub-link 4a, which is affected by a hardware malfunction (*Appendix B*). The correlation between the classifiers of sub-links belonging to different CMLs is lower but still reaches high values ranging between r = 0.57 and r = 0.84. The correlation of CML classifiers to the classifiers based on rain gauges is, on average, slightly lower (r = 0.57–0.67).

The evaluation of dry-wet weather classification is only approximate because tipping bucket rain gauges are unable to detect the exact beginning or end of a rain event. Visual inspection of time series reveals that disagreement between rain gauges and CMLs ~~occur~~occurs most commonly during dew events and during periods of low temperature where mixed or snow events probably occur. Although sensitivity to dew events can be increased by optimizing the parameters of the algorithm, dew events have similar dynamics as changes in air humidity as they are both dependent on temperature. Thus, other methods also considering observations of neighboring CMLs (Overeem et al., 2011) might be more appropriate for the dry-wet weather classification used ~~for the separation of~~to separate attenuation caused by water vapor.

Appendix B – Hardware-related artifacts

There have been three types of hardware-related artifacts identified (visually) in the Prague data (Fig. B1): a) a sudden change in L_t, b) long-term gradual L_t drift, and c) 'degraded resolution'. 'Degraded resolution' is defined as a behavior where *tx* and *rx* change with a considerably lower frequency than is common with other CMLs. The degraded resolution can be easily recognized visually as a time series with no signal fluctuation within intervals of several hours.

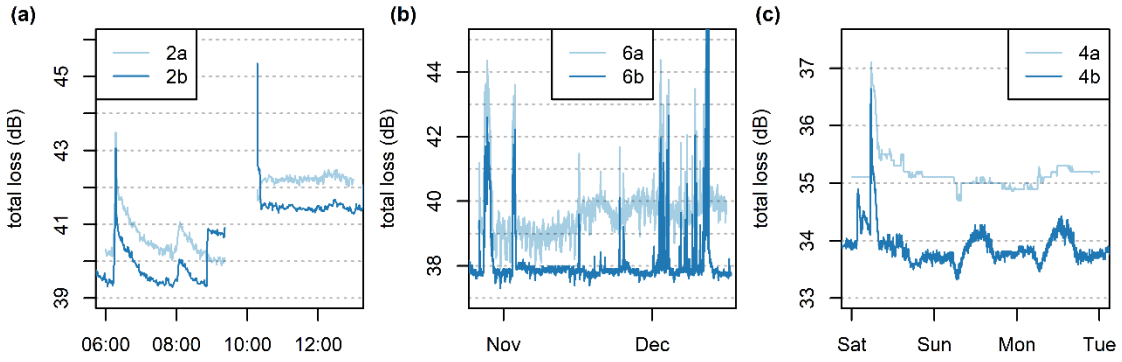

Figure B1: Demonstration of hardware related artifacts (a) sudden change in the baseline of CML 2, (b) baseline drift of sub-link 6a and (c) degraded resolution of sub-link 4a.

The sudden change in L_t of about 2 dB occurred on CML 2 on both sub-links (Fig. B1a). The change in baseline level was proceeded by approx. two hours of an outage. The long-term gradual drift of L_t occurred on sub-link 6a (Fig. B1b). L_t levels observed during dry weather increased gradually, on average, by about 1.5 dB during the experimental period. Finally, sub-link 4a was affected during the whole experimental period by a degraded resolution (Fig. B1c). Interestingly, the degraded resolution was more pronounced during dry weather periods than rainy ones.

In general, attenuation levels during dry weather are relatively stable with respect to long-term drift (in the order of weeks). It holds for all CMLs except the 73 GHz sub-link of CML 6, which has dry weather attenuation levels of about 1.5 dB higher at the end of the period compared to the beginning (Fig. B1b). The most significant fluctuations in the baseline occur during dew events when water film forming on the CML antennas causes wet antenna attenuation (section 3.4~~.3~~). The baseline fluctuations related to water vapor are presented in section 4.1 (Fig. ~~5~~7).

The hardware~~–~~related artifacts identified in the E-band attenuation time series are similar to those occurring on 15–40 GHz CMLs. The 'degraded resolution' can be ~~identified~~determined easily by analyzing attenuation variability within (sub)hourly subsets. Detecting (and correcting for) the sudden change in attenuation level will be especially challenging in operation mode when attenuation needs to be processed in real-time. Long-term drift can be captured very well and corrected using a median moving window with a size of one week. Such a ~~size~~width of window is sufficiently long to not include more than 50 % of wet weather records into the window at any time step in the temperate climate

Supplement link (will be included by Copernicus).

Code and data availability. The code for Prague data analysis and Prague data are publically available at Zenodo repository DOI 10.5281/zenodo.3632095. Duebendorf data (disdrometer observations) and the code are available upon request from the corresponding author.

Author contribution. MF and VB. designed the study layout. Data was collected by MF, VB and MD. Analysis was performed by MF with contribution of MD, MG, and PV. MF prepared the manuscript with contribution of all co-authors.

Competing interests. The authors declare that they have no conflict of interest.

~~*Acknowledgements.*~~*Acknowledgments.* This work was supported by the projects of Czech Science Foundation (GACR) No. 17-16389S and No. 20-14151J. We would like to thank T-Mobile Czech Republic a.s. for kindly providing us CML data and specifically to Pavel Kubík, for assisting with our numerous requests. Special thanks are extended to Prazska vodohospodarska spolecnost a.s. for providing rainfall data from their rain gauge network and Prazske vodovody a kanalizace, a.s. who carefully maintained the rain gauges. Last~~,~~ but not least, we would like to thank Eawag for supporting COMMON project and Dr. Christian Chwala from Karlsruhe Institute of Technology (KIT) and University of Augsburg for supporting our analysis by calculating extinction cross-sections and providing Python implementation of Liebe model for calculating attenuation due to water vapor.

References

Atlas, D. and Ulbrich, C. W.: Path- and Area-Integrated Rainfall Measurement by Microwave Attenuation in the 1–3 cm Band, J. Appl. Meteor., 16(12), 1322–1331, doi:10.1175/1520-0450(1977)016<1322:PAAIRM>2.0.CO;2, 1977.

Berne, A. and Uijlenhoet, R.: Path-averaged rainfall estimation using microwave links: Uncertainty due to spatial rainfall variability, Geophys. Res. Lett., 34(7), L07403, doi:10.1029/2007GL029409, 2007.

Chwala, C.: Precipitation and humidity observation using a microwave transmission experiment and commercial microwave links, [online] Available from: https://opus.bibliothek.uni-augsburg.de/opus4/frontdoor/index/index/docId/37908 (Accessed 2 December 2019), 2017.

Chwala, C. and Kunstmann, H.: Commercial microwave link networks for rainfall observation: Assessment of the current status and future challenges, Wiley Interdisciplinary Reviews: Water, 6(2), e1337, doi:10.1002/wat2.1337, 2019.

Chwala, C., Keis, F. and Kunstmann, H.: Real-time data acquisition of commercial microwave link networks for hydrometeorological applications, Atmos. Meas. Tech., 9(3), 991–999, doi:10.5194/amt-9-991-2016, 2016.

David, N., Alpert, P. and Messer, H.: Technical Note: Novel method for water vapour monitoring using wireless communication networks measurements, Atmospheric Chemistry and Physics, 9(7), 2413–2418, doi:https://doi.org/10.5194/acp-9-2413-2009, 2009.

David, N., Sendik, O., Rubin, Y., Messer, H., Gao, H. O., Rostkier-Edelstein, D. and Alpert, P.: Analyzing the ability to reconstruct the moisture field using commercial microwave network data, Atmospheric Research, 219, 213–222, doi:10.1016/j.atmosres.2018.12.025, 2019.

Ericsson: Ericsson Microwave Outlook, [online] Available from: https://www.ericsson.com/assets/local/microwave-outlook/documents/ericsson-microwave-outlook-report-2016.pdf (Accessed 15 July 2017), 2016.

Ericsson: Ericsson Microwave Outlook Report - 2018, [online] Available from: https://www.ericsson.com/en/reports-and-papers/microwave-outlook/reports/2018 (Accessed 10 December 2019), 2018.

Ericsson: Ericsson Microwave Outlook Report - 2019, [online] Available from: https://www.ericsson.com/en/reports-and-papers/microwave-outlook/reports/2019 (Accessed 10 December 2019), 2019.

Fencl, M., Dohnal, M., Rieckermann, J. and Bareš, V.: Gauge-adjusted rainfall estimates from commercial microwave links, Hydrol. Earth Syst. Sci., 21(1), 617–634, doi:10.5194/hess-21-617-2017, 2017.

Fencl, M., Valtr, P., Kvičera, M. and Bareš, V.: Quantifying Wet Antenna Attenuation in 38-GHz Commercial Microwave Links of Cellular Backhaul, IEEE Geoscience and Remote Sensing Letters, 16(4), 514–518, doi:10.1109/LGRS.2018.2876696, 2019.

Fencl, M., Dohnal, M. and Bareš, V.: Raw and preprocessed data for the paper Atmospheric Observations with E-band Microwave Links – Challenges and Opportunities, , doi:10.5281/zenodo.3632095, 2020.

~~Fujiwara, M.: Raindrop-size Distribution from Individual Storms, J. Atmos. Sci., 22(5), 585–591, doi:10.1175/1520-0469(1965)022<0585:RSDFIS>2.0.CO;2, 1965.~~

Hansryd, J., Li, Y., Chen, J. and Ligander, P.: Long term path attenuation measurement of the 71–76 GHz band in a 70/80 GHz microwave link, in Proceedings of the Fourth European Conference on Antennas and Propagation, pp. 1–4., 2010.

Hong, E. S., Lane, S., Murrell, D., Tarasenko, N. and Christodoulou, C.: Mitigation of Reflector Dish Wet Antenna Effect at 72 and 84 GHz, IEEE Antennas and Wireless Propagation Letters, 16, 3100–3103, doi:10.1109/LAWP.2017.2762519, 2017.

Humphrey, M. D., Istok, J. D., Lee, J. Y., Hevesi, J. A. and Flint, A. L.: A New Method for Automated Dynamic Calibration of Tipping-Bucket Rain Gauges, J. Atmos. Oceanic Technol., 14(6), 1513–1519, doi:10.1175/1520-0426(1997)014<1513:ANMFAD>2.0.CO;2, 1997.

Internationale Fernmelde-Union, Ed.: Handbook radiowave propagation information for desining terrestrial point-to-point links, Ed. 2008., ITU, Geneva., 2009.

ITU-R: ITU-R P.838-3, [online] Available from: http://www.itu.int/dms_pubrec/itu-r/rec/p/R-REC-P.838-3-200503-I!!PDF-E.pdf, 2005.

ITU-R: RECOMMENDATION ITU-R P.676-12 - Attenuation by atmospheric gases and related effects, [online] Available from: https://www.itu.int/dms_pubrec/itu-r/rec/p/R-REC-P.676-12-201908-I!!PDF-E.pdf, 2019.

Jaffrain, J. and Berne, A.: Experimental Quantification of the Sampling Uncertainty Associated with Measurements from PARSIVEL Disdrometers, J. Hydrometeor., 12(3), 352–370, doi:10.1175/2010JHM1244.1, 2010.

Jaffrain, J. and Berne, A.: Quantification of the Small-Scale Spatial Structure of the Raindrop Size Distribution from a Network of Disdrometers, J. Appl. Meteor. Climatol., 51(5), 941–953, doi:10.1175/JAMC-D-11-0136.1, 2012.

Leijnse, H., Uijlenhoet, R. and Stricker, J. N. M.: Rainfall measurement using radio links from cellular communication networks, Water Resour. Res., 43(3), W03201, doi:10.1029/2006WR005631, 2007.

Leijnse, H., Uijlenhoet, R. and Stricker, J. N. M.: Microwave link rainfall estimation: Effects of link length and frequency, temporal sampling, power resolution, and wet antenna attenuation, Advances in Water Resources, 31(11), 1481–1493, doi:10.1016/j.advwatres.2008.03.004, 2008.

Leinonen, J.: High-level interface to T-matrix scattering calculations: architecture, capabilities and limitations, Opt. Express, OE, 22(2), 1655–1660, doi:10.1364/OE.22.001655, 2014.

Leth, T. C. van, Overeem, A., Leijnse, H. and Uijlenhoet, R.: A measurement campaign to assess sources of error in microwave link rainfall estimation, Atmospheric Measurement Techniques, 11(8), 4645–4669, doi:https://doi.org/10.5194/amt-11-4645-2018, 2018.

Leth, T. C. van, Leijnse, H., Overeem, A. and Uijlenhoet, R.: Estimating raindrop size distributions using microwave link measurements, Atmospheric Measurement Techniques Discussions, 1–27, doi:https://doi.org/10.5194/amt-2019-51, 2019.

Liebe, H. J., Hufford, G. A. and Cotton, M. G.: Propagation modeling of moist air and suspended water/ice particles at frequencies below 1000 GHz. [online] Available from: http://adsabs.harvard.edu/abs/1993apet.agar.....L (Accessed 17 October 2019), 1993.

Luini, L., Roveda, G., Zaffaroni, M., Costa, M. and Riva, C.: EM wave propagation experiment at E band and D band for 5G wireless systems: Preliminary results, in 12th European Conference on Antennas and Propagation (EuCAP 2018), pp. 1–5., 2018.

Mancini, A., Lebrón, R. M. and Salazar, J. L.: The Impact of a Wet S-Band Radome on Dual-Polarized Phased-Array Radar System Performance, IEEE Transactions on Antennas and Propagation, 67(1), 207–220, doi:10.1109/TAP.2018.2876733, 2019.

Messer, H., Zinevich, A. and Alpert, P.: Environmental Monitoring by Wireless Communication Networks, Science, 312(5774), 713–713, doi:10.1126/science.1120034, 2006.

Minda, H. and Nakamura, K.: High Temporal Resolution Path-Average Rain Gauge with 50-GHz Band Microwave, Journal of Atmospheric and Oceanic Technology, 22(2), 165–179, doi:10.1175/JTECH-1683.1, 2005.

Mishchenko, M. I. and Travis, L. D.: Capabilities and limitations of a current FORTRAN implementation of the T-matrix method for randomly oriented, rotationally symmetric scatterers, Journal of Quantitative Spectroscopy and Radiative Transfer, 60(3), 309–324, 1998.

Moroder, C., Siart, U., Chwala, C. and Kunstmann, H.: Modeling of Wet Antenna Attenuation for Precipitation Estimation From Microwave Links, IEEE Geoscience and Remote Sensing Letters, 17(3), 386–390, doi:10.1109/LGRS.2019.2922768, 2020.

Olsen, R., Rogers, D. and Hodge, D.: The aRbrelation in the calculation of rain attenuation, IEEE Transactions on Antennas and Propagation, 26(2), 318–329, doi:10.1109/TAP.1978.1141845, 1978.

Ostrometzky, J., Raich, R., Bao, L., Hansryd, J. and Messer, H.: The Wet-Antenna Effect—A Factor to be Considered in Future Communication Networks, IEEE Transactions on Antennas and Propagation, 66(1), 315–322, doi:10.1109/TAP.2017.2767620, 2018.

Overeem, A., Leijnse, H. and Uijlenhoet, R.: Measuring urban rainfall using microwave links from commercial cellular communication networks, Water Resources Research, 47(12), doi:10.1029/2010WR010350, 2011.

Pruppacher, H. R. and Beard, K. V.: A wind tunnel investigation of the internal circulation and shape of water drops falling at terminal velocity in air, Quarterly Journal of the Royal Meteorological Society, 96(408), 247–256, doi:10.1002/qj.49709640807, 1970.

Schleiss, M. and Berne, A.: Identification of Dry and Rainy Periods Using Telecommunication Microwave Links, IEEE Geoscience and Remote Sensing Letters, 7(3), 611–615, doi:10.1109/LGRS.2010.2043052, 2010.

Schleiss, M., Rieckermann, J. and Berne, A.: Quantification and Modeling of Wet-Antenna Attenuation for Commercial Microwave Links, IEEE Geoscience and Remote Sensing Letters, 10(5), 1195–1199, doi:10.1109/LGRS.2012.2236074, 2013.

~~Ulbrich, C. W.: Natural Variations in the Analytical Form of the Raindrop Size Distribution, J. Climate Appl. Meteor., 22(10), 1764–1775, doi:10.1175/1520-0450(1983)022<1764:NVITAF>2.0.CO;2, 1983.~~

Valtr, P., Pechac, P., Kvicera, V. and Grabner, M.: Estimation of the Refractivity Structure of the Lower Troposphere From Measurements on a Terrestrial Multiple-Receiver Radio Link, IEEE Transactions on Antennas and Propagation, 59(5), 1707–1715, doi:10.1109/TAP.2011.2122234, 2011.

Wang, Z., Schleiss, M., Jaffrain, J., Berne, A. and Rieckermann, J.: Using Markov switching models to infer dry and rainy periods from telecommunication microwave link signals, Atmospheric Measurement Techniques, 5(7), 1847–1859, doi:10.5194/amt-5-1847-2012, 2012.

Woodhouse, I. H.: Introduction to microwave remote sensing, CRC press., 2017.